

การดูดซับของแก๊สขนาดเล็กในโครงข่ายอินทรีย์โลหะชนิด MIL-127



นายปวีร์ พงษ์สัจจนกุล

จุฬาลงกรณ์มหาวิทยาลัย

CHULALONGKORN UNIVERSITY

บทคัดย่อและแฟ้มข้อมูลฉบับเต็มของวิทยานิพนธ์ตั้งแต่ปีการศึกษา 2554 ที่ให้บริการในคลังปัญญาจุฬาฯ (CUIR)

เป็นแฟ้มข้อมูลของนิสิตเจ้าของวิทยานิพนธ์ ที่ส่งผ่านทางบัณฑิตวิทยาลัย

The abstract and full text of theses from the academic year 2011 in Chulalongkorn University Intellectual Repository (CUIR) are the thesis authors' files submitted through the University Graduate School.

วิทยานิพนธ์นี้เป็นส่วนหนึ่งของการศึกษาตามหลักสูตรปริญญาวิทยาศาสตรมหาบัณฑิต

สาขาวิชาเคมี ภาควิชาเคมี

คณะวิทยาศาสตร์ จุฬาลงกรณ์มหาวิทยาลัย

ปีการศึกษา 2559

ลิขสิทธิ์ของจุฬาลงกรณ์มหาวิทยาลัย

ADSORPTION OF SMALL GASES IN MIL-127 METAL ORGANIC FRAMEWORKS

Mr. Pavee Pongsajanukul



A Thesis Submitted in Partial Fulfillment of the Requirements
for the Degree of Master of Science Program in Chemistry

Department of Chemistry

Faculty of Science

Chulalongkorn University

Academic Year 2016

Copyright of Chulalongkorn University

Thesis Title	ADSORPTION OF SMALL GASES IN MIL-127 METAL ORGANIC FRAMEWORKS
By	Mr. Pavee Pongsajanukul
Field of Study	Chemistry
Thesis Advisor	Associate Professor Vudhichai Parasuk, Ph.D.
Thesis Co-Advisor	Tatiya Chokbunpiam, Ph.D.

Accepted by the Faculty of Science, Chulalongkorn University in Partial
Fulfillment of the Requirements for the Master's Degree

..... Dean of the Faculty of Science
(Associate Professor Polkit Sangvanich, Ph.D.)

THESIS COMMITTEE

..... Chairman
(Assistant Professor Varawut Tangpasuthadol, Ph.D.)

..... Thesis Advisor
(Associate Professor Vudhichai Parasuk, Ph.D.)

..... Thesis Co-Advisor
(Tatiya Chokbunpiam, Ph.D.)

..... Examiner
(Assistant Professor Somsak Pianwanit, Ph.D.)

..... External Examiner
(Assistant Professor Tawun Remsungnen, Ph.D.)

ปวีร์ พงษ์สัจจนกุล : การดูดซับของแก๊สขนาดเล็กในโครงข่ายอินทรีย์โลหะชนิด MIL-127 (ADSORPTION OF SMALL GASES IN MIL-127 METAL ORGANIC FRAMEWORKS) อ. ที่ปรึกษาวิทยานิพนธ์หลัก: รศ. ดร. วุฒิชัย พาราสุข, อ. ที่ปรึกษาวิทยานิพนธ์ร่วม: ดร. ตติยา โชคบุญเปี่ยม, 66 หน้า.

วัสดุจากสถาบันวิจัยลาวัวซีเยร์ชนิด 127 (MIL-127) จัดเป็นวัสดุโครงข่ายอินทรีย์โลหะ (MOF) ชนิดหนึ่ง ซึ่งได้มีการนำวัสดุชนิดนี้มาประยุกต์อย่างหลากหลาย เช่น ใช้กักเก็บและแยกแก๊ส ใช้เป็นตัวเร่งปฏิกิริยา และประยุกต์กับระบบทางชีวภาพ โดย MIL-127 ประกอบด้วยไตรเมอร์ของเหล็ก และสาร 3,3',5,5'-เอโซเบนซีนเตตระคาร์บอกซิเลท แอนไอออนทำหน้าที่เป็นตัวเชื่อม (linker) งานวิจัยนี้ใช้เทคนิคการจำลองแบบกิบส์ของซอมเบลมอนติคาร์โล (Gibbs Ensemble Monte Carlo simulation, GEMC) และการจำลองแบบทางพลวัตเชิงโมเลกุล (Molecular Dynamics simulation, MD) เพื่อศึกษาพฤติกรรมการดูดซับและการแพร่ของโมเลกุลแก๊สขนาดเล็กใน MIL-127 โครงสร้างของ MIL-127 ที่ใช้ในงานวิจัยนี้ได้จากข้อมูลเอกซเรย์ดิฟแฟรคชัน (x-ray diffraction) เพื่อทำการจำลองต้องมีการเลือกชุดพารามิเตอร์ที่เหมาะสมมาทำการคำนวณ โดยชุดพารามิเตอร์เหล่านั้นได้มาจากการคำนวณทางเคมีควอนตัมและงานวิจัยที่เกี่ยวข้อง ผลที่ได้จากการจำลองนี้ได้ถูกนำมาเปรียบเทียบกับผลการทดลองจากห้องปฏิบัติการโดยการเปรียบเทียบไอโซเทอร์มการดูดซับ (adsorption isotherm) ของโมเลกุลแก๊สคาร์บอนไดออกไซด์และคาร์บอนมอนอกไซด์ในวัสดุชนิดนี้เพื่อเลือกพารามิเตอร์ที่เหมาะสมสำหรับการคำนวณฟังก์ชันการกระจายเชิงรัศมี (radial distribution function, RDF) และฟังก์ชันหนาแน่นความน่าจะเป็น (probability density) เพื่ออธิบายพฤติกรรมของโมเลกุลแก๊สขนาดเล็กในวัสดุ MIL-127 จากการจำลองแบบพบว่า ตำแหน่งดูดซับที่ชอบของแก๊สคาร์บอนไดออกไซด์อยู่ที่บริเวณโลหะอินทรีย์ ซึ่งตรงกันข้ามกับตำแหน่งดูดซับที่ชอบของแก๊สคาร์บอนมอนอกไซด์ที่อยู่บริเวณสารอินทรีย์ ในขั้นตอนสุดท้าย ได้เลือกชุดพารามิเตอร์ที่เหมาะสมสำหรับการคำนวณ สำหรับศึกษาสมบัติทางโครงสร้างและการแพร่ของโมเลกุลแก๊สในวัสดุโครงข่ายอินทรีย์โลหะนี้ โดยค่าสัมประสิทธิ์การแพร่ในตัวเองของแก๊สคาร์บอนไดออกไซด์อยู่ในช่วงระหว่าง $1-3 \times 10^{-9}$ เมตร²/วินาที และค่าสัมประสิทธิ์การแพร่ในตัวเองของแก๊สคาร์บอนมอนอกไซด์อยู่ในช่วงระหว่าง $4-14 \times 10^{-9}$ เมตร²/วินาที

ภาควิชา	เคมี	ลายมือชื่อนิสิต
สาขาวิชา	เคมี	ลายมือชื่อ อ. ที่ปรึกษาหลัก
ปีการศึกษา	2559	ลายมือชื่อ อ. ที่ปรึกษาร่วม

5772053123 : MAJOR CHEMISTRY

KEYWORDS: MATERIAL OF INSTITUT LAVOISIER -127 (MIL-127) / ADSORPTION /
DIFFUSION / COMPUTATIONAL CALCULATIONS

PAVEE PONGSAJANUKUL: ADSORPTION OF SMALL GASES IN MIL-127 METAL
ORGANIC FRAMEWORKS. ADVISOR: ASSOC. PROF. VUDHICHAJ PARASUK, Ph.D.,
CO-ADVISOR: TATIYA CHOKBUNPIAM, Ph.D., 66 pp.

Material of Institut Lavoisier -127 (MIL-127) is one of series of porous metal-organic frameworks (MOFs) that have many potential applications such as gas storage and separation, catalysis, and biological applications. MIL-127 is composed of trimers of iron(III) and 3,3',5,5' - azobenzenetetracarboxylate anions. To gain insight into the adsorption behavior and the dynamic behavior of small gases in MIL-127, we carried out Gibbs Ensemble Monte Carlo (GEMC) and Molecular Dynamics (MD) simulations. Firstly, the structure of MIL-127(Fe) was constructed from XRD result. Force field parameters were carefully selected. Different parameter sets from both quantum calculations and literatures have been employed. Their results were compared with each other and with experiments to find the one that can well reproduce the adsorption isotherm of small gases in MIL-127(Fe). Radial distribution functions (RDFs) and probability density were done to elucidate behavior of small gases. From simulations, the preferential adsorption sites of carbon dioxide is around the metal cluster zone of MIL-127(Fe) in contrast to adsorption sites of carbon monoxide which prefers to adsorb around organic linker zone. Finally, selected parameters were used to investigate the structure and self-diffusion of the guest molecules in the MIL-127(Fe). The self-diffusion coefficient of carbon dioxide is in the range of $1-3 \times 10^{-9}$ m²/s and the self-diffusion coefficient of carbon monoxide is in the range of $4-14 \times 10^{-9}$ m²/s.

Department: Chemistry

Field of Study: Chemistry

Academic Year: 2016

Student's Signature

Advisor's Signature

Co-Advisor's Signature

ACKNOWLEDGEMENTS

The thesis for master degree could not have been completed without the good instruction, encouragement as well support throughout three years of study at Chulalongkorn University.

I would like to gratefully and sincerely thank my advisor, Assoc. Prof. Dr. Vudhichai Parasuk and my co-advisor, Dr. Tatiya Chokbunpiam for not only teaching, giving a useful guidance but also encouraging me during the time of my research.

I would like to thank my thesis committee, Asst. Prof. Dr. Varawut Tangpasuthadol, Asst. Prof. Dr. Somsak Pianwanit, and Asst. Prof. Dr. Tawun Remsungnen for giving useful suggestions. I would also like to thank Priv-Doz. Dr. Siegfried Fritzsche for giving several suggestions and helping me improve my language.

In addition, I would like to thank Prof. Dr. Suttichai Assabumrungrat, Assoc. Prof. Dr. Thiti Bovornratanaraks and Dr. Suwimol Wongsakulphasatch for giving helpful suggestions and collaborating with my first publication.

I most expressly special thank my family, my friends and Dr. Tatiya Chokbunpiam for all their supports and cheering me up throughout the period of my study.

Finally, I would like to thank the Development and Promotion of Science and Technology Talents Project (DPST) for financial support and the Computational Chemistry Unit Cell (CCUC) at Department of Chemistry, Faculty of Science, Chulalongkorn University for computer resources.

In remembrance of His Majesty King Bhumibol Adulyadej (1927-2016), for his life-time dedication to Thailand.

CONTENTS

	Page
THAI ABSTRACT	iv
ENGLISH ABSTRACT	v
ACKNOWLEDGEMENTS	vi
CONTENTS	vii
LIST OF FIGURES	1
LIST OF TABLES	4
CHAPTER I INTRODUCTION.....	5
1.1 Research rationale	5
1.2 Material of Institut Lavoisier-127 (MIL-127).....	6
1.3 Applications.....	7
1.3.1 Gas storage.....	8
1.3.2 Gas separation	8
1.3.3 Catalysis	8
1.4 Literature reviews.....	8
1.5 Scope of this research	10
CHAPTER II THEORY BACKGROUND	11
2.1 Quantum Mechanics	11
2.1.1 Schrödinger equation.....	11
2.1.2 Born-Oppenheimer approximation	12
2.1.3 Hartree-Fock method.....	14
2.1.4 Basis sets.....	14
2.2 Simulations.....	16

	Page
2.2.1 Ensemble.....	17
2.2.2 Molecular mechanics and Force Field parameters	18
2.2.3 Monte Carlo (MC) simulations.....	20
2.2.3.1 Gibbs ensemble Monte Carlo (GEMC) simulations	20
2.2.4 Molecular Dynamics (MD) simulations	21
2.2.4.1 Integration algorithms	22
2.2.5 Periodic Boundary Condition.....	24
2.2.6 Radial Distribution Functions (RDFs)	25
2.2.7 Molecular diffusion.....	26
CHAPTER III CALCULATION DETAILS	27
3.1 Quantum Mechanical calculations.....	27
3.2 Simulations.....	28
3.2.1 Force fields.....	28
3.2.2 Gibbs ensemble Monte Carlo (GEMC) simulations details	31
3.2.3 Molecular Dynamics (MD) simulations details	33
CHAPTER IV RESULTS AND DISCUSSION	35
4.1 Quantum Mechanical calculations.....	35
4.2 Carbon dioxide in MIL-127	36
4.2.1 Adsorption isotherms	36
4.2.2 Radial Distribution Functions (RDF)	37
4.2.3 Probability density.....	41
4.2.4 Site of the lowest potential energy	42
4.2.5 Self-Diffusion coefficient from Molecular Dynamics (MD) simulations	43

	Page
4.3 Carbon monoxide in MIL-127	45
4.3.1 Adsorption isotherms	45
4.3.2 Radial Distribution Functions (RDFs)	46
4.3.3 Probability density	47
4.3.4 Site of the lowest potential energy	48
4.3.5 Self-Diffusion coefficient from Molecular Dynamics (MD) simulations	49
CHAPTER V CONCLUSIONS	51
REFERENCES	52
APPENDIX	61
VITA	66



LIST OF FIGURES

Page

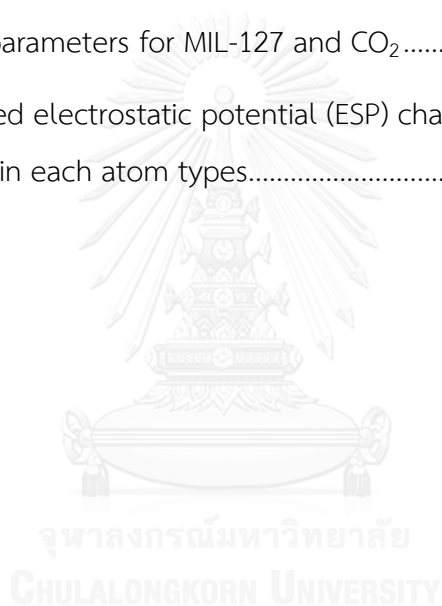
Figure 1 (a) Schematic representation the structure of MIL-127(Fe) (b) Trimers of iron (III) (c) 3,3',5,5'-azobenzenetetracarboxylate (Tazb). The atoms of carbon, hydrogen, oxygen, nitrogen and trimers of iron (III) are shown by grey, white, red, blue and purple polyhedral, respectively.....	7
Figure 2 The interatomic interactions in molecular mechanics [38].....	18
Figure 3 The Lennard-Jones potential use to describe interatomic potential of molecule. [39].....	19
Figure 4 Schematic illustration of movement in Gibbs ensemble Monte Carlo (GEMC) simulations. [42].....	21
Figure 5 Schematic representation of Molecular dynamics simulation diagram....	23
Figure 6 Schematic represent periodic boundary conditions in two dimensions [43].....	24
Figure 7 Schematic explanation of the radial distribution functions [45].....	25
Figure 8 Two structures used to estimate the electrostatic potential (ESP) charges for organic linker (left) and metal cluster (right) in MIL-127(Fe).	27
Figure 9 The structure of MIL-127(Fe) as constructed from XRD data composing of metal cluster and organic linker. The carbon, hydrogen, oxygen, nitrogen and iron atoms are shown by grey, white, red, blue and purple colors, respectively. In addition, the label of atom types in the MIL-127(Fe) are displayed.....	28
Figure 10 Adsorption isotherms of carbon dioxide in MIL-127(Fe) compared with experimental results using UFF for MIL-127(Fe) and FF1 and FF2 for carbon dioxide (a) and using LJ parameters from Babarao <i>et. al.</i> [53] for MIL-127(Fe) and FF2 for carbon dioxide (b)	37
Figure 11 RDF's between carbon of carbon dioxide and 3 atom types in MIL-127(Fe) (a, b, c) and RDF between oxygen of carbon dioxide and 3 atom types in	

MIL-127(Fe) (d, e, f) at 0.14, 1.04, and 1.71 bar. All graphs were obtained from GEMC simulations.	39
Figure 12 RDF between carbon of carbon dioxide and MIL-127(Fe) (a-f) RDF between oxygen of carbon dioxide and MIL-127(Fe) (g-l) at concentration 5, 10, 15, 20, 25 and 30 molecules/unit cell, respectively. All graphs obtained from MD simulations.	40
Figure 13 A comparison of RDF between GEMC and MD simulations. The figure on the left side show RDF between carbon of carbon dioxide and 3 atom types in MIL-127(Fe) whereas the figure on the right side show RDF between oxygen of carbon dioxide and 3 atom types in MIL-127(Fe). GEMC data and MD data were obtained at the concentration around 5 molecule/unit cell.	41
Figure 14 Probability density of carbon dioxide in MIL-127(Fe) obtained from GEMC simulations at pressure (a) 0.14 bar (b) 1.04 bar and (c) 1.71 bar, respectively.	41
Figure 15 The position and orientation of a virtual molecule at the site and orientation of the lowest potential energy from GEMC simulations in top views (left) and side views (right) at pressure (a) 0.14 bar (top) (b) 1.04 bar (middle) and (c) 1.71 bar (bottom), are shown, respectively. The other molecules are not shown.	43
Figure 16 The self-diffusion coefficients of carbon dioxide molecules in MIL-127(Fe) at the different concentrations.	44
Figure 17 Adsorption isotherm of carbon monoxide in MIL-127(Fe) compared with experimental results using FF1, FF2, FF3, FF4 and FF5 for carbon monoxide and using LJ parameters from Babarao et al. [53] for MIL-127(Fe) (a) and the adsorption isotherm using FF1 for carbon monoxide with applied charges (b).	45
Figure 18 RDF's between carbon of carbon monoxide and 5 atom types in MIL-127(Fe) (a, b, c) and RDF between oxygen of carbon monoxide and 5 atom types in MIL-127(Fe) (d, e, f) at 0.08, 0.49, and 1.07 bar. All graphs were obtained from GEMC simulations.	46

Figure 19 Probability density of carbon monoxide in MIL-127(Fe) obtained from GEMC simulations at pressure (a) 0.08 bar (b) 0.49 bar and (c) 1.07 bar, respectively.....	47
Figure 20 The position and orientation of a virtual molecule at the site and orientation of the lowest potential energy from GEMC simulations at pressure (a) 0.08 bar (b) 0.49 bar and (c) 1.07 bar, respectively. The other molecules are not shown.....	48
Figure 21 The self-diffusion coefficients of carbon monoxide molecules in MIL-127(Fe) at the different concentrations.....	49
Figure 22 Adsorption isotherm between MIL-127(Fe) and carbon dioxide compared with experiment. (a) After adjusted the charge of CO ₂ , (b) after adjusted the charge of MIL-127(Fe).....	61
Figure 23 RDF of carbon dioxide in MIL-127(Fe) at concentration 5, 10, 15, 20, 25 and 30 molecules/unit cell, respectively. All graphs obtained from MD simulations.....	61
Figure 24 Two structures used to estimate the electrostatic potential (ESP) charges for organic linker (left) and metal cluster (right) in MIL-127(Fe).	63
Figure 25 The mean square displacement of carbon dioxide in MIL-127(Fe) obtained from NVT ensemble.	63
Figure 26 The mean square displacement of carbon dioxide in MIL-127(Fe) obtained from NVE ensemble.	64
Figure 27 The mean square displacement of carbon monoxide in MIL-127(Fe) obtained from NVT ensemble.	65

LIST OF TABLES

	Page
Table 1 The Lennard-Jones potential parameters for MIL-127(Fe)	30
Table 2 Force field 1 (FF1) of carbon dioxide [54]	30
Table 3 Force field 2 (FF2) of carbon dioxide [55]	30
Table 4 Force field parameters for carbon monoxide.	31
Table 5 The adjusted ESP charge of each atom types in MIL-127(Fe).....	35
Table 6 Force Field parameters for MIL-127 and CO ₂	36
Table 7 The calculated electrostatic potential (ESP) charges to estimate the atomic partial charge in each atom types.....	62



CHAPTER I

INTRODUCTION

1.1 Research rationale

Carbon dioxide (CO₂) is a colorless and odorless gas which occurs in the atmosphere from natural sources or is emitted from human activities. For instance it is created by the combustion of fossil fuels or by industry and it is enhanced by the extensive deforestation. This leads to the global environment problems due to the increase of the greenhouse gases. [1] Likewise carbon dioxide, carbon monoxide (CO) is a poisonous gas that has no smell or taste. It can be found in the air when the exhaust from incomplete combustion is occurred, for example, burning fuel in cars or small engines. Carbon monoxide have been reported to make you unwell if we breathing it in high levels.

Many countries have attempted to reduce the toxic gases in the atmosphere. In chemical processes, controlling the gas emission by capture or separation, gas storage, etc. become a challenging issue. [2] Therefore, porous material becomes the promising alternative material, which can be used to eliminate this problems.

Metal Organic Frameworks (MOFs) or porous coordination networks are porous solid materials derived from metal oxide clusters connected by organic linkers. [3] The formation of MOFs originate from self-assembly with well-defined pore size and desired chemical functional. MOFs have been developed over a decade due to the fact that they have many attractive properties. MOFs provide a large surface areas, tunable pore sizes and topologies. Due to an interesting performance of MOFs, they were applied for potential applications such as gas storage, gas separation, catalysis and biological applications. Material of Institut Lavoisiers (MILs) is one type of MOFs. The interesting features and the properties of MILs are similar to other MOFs. Around

150 types of MILs were designed as crystalline porous materials. In this work, we focused on MIL-127(Fe) which consist of trimers of iron (III) and 3,3',5,5'-azobenzene-tetracarboxylate anion as organic linkers. MIL-127(Fe) exhibits the square octahedral topology. The structure contains two types of pores: the cage (~10 Å) and the 1D channel (~6 Å) or only 1D channel was assumed that the windows giving accessible through narrow apertures (~4 Å). So it is suitable for using in the applications such as storage or separation of the small gases like CO or CO₂.

A lot of experimental studies have been shown the potential applications of MIL-127(Fe). Beside experiments, computational methods are useful to gain insight into the adsorption and diffusion behaviors of guest molecules. A lot of studies use Monte Carlo simulations to get deeper understanding of adsorption mechanisms (see *e.g.* [4-8]) while molecular dynamic (MD) simulations are used to study diffusivities of gas molecules in MOFs (see *e.g.* [6-10]) However, to our knowledge there is no theoretical study of adsorption and diffusion behaviors of small gases in MIL-127 until now.

In this work, adsorption and diffusion behaviors of CO and CO₂ in MIL-127(Fe) were investigated using GEMC simulations and MD simulations. This research is expected to give insights in the behavior of small gases inside MIL-127(Fe).

1.2 Material of Institut Lavoisier-127 (MIL-127)

Material of Institut Lavoisier -127 (MIL-127) is one of porous metal organic frameworks. The structure of MIL-127(Fe) is composed of trimers of iron (III) and 3,3',5,5'- azobenzene-tetracarboxylate anions. The trimers of iron (III) sharing one central μ_3 – oxo anion to form trimeric building blocks. Generally, MIL-127(Fe) structure was built in a form of square octahedral topology, sometimes we called soc-MOF(Fe).

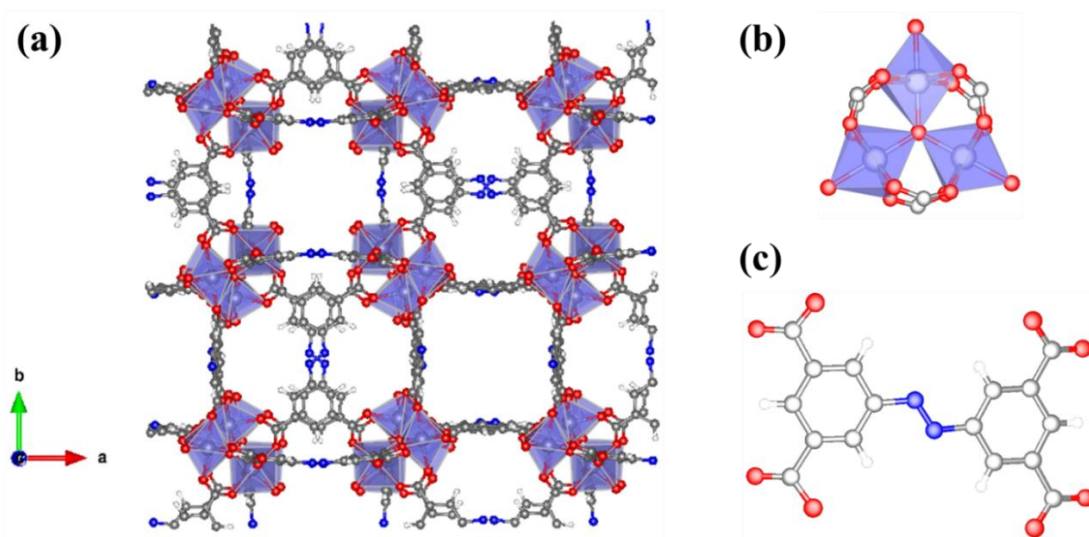


Figure 1 (a) Schematic representation the structure of MIL-127(Fe) (b) Trimers of iron (III) (c) 3,3',5,5'-azobenzene tetracarboxylate (Tazb). The atoms of carbon, hydrogen, oxygen, nitrogen and trimers of iron (III) are shown by grey, white, red, blue and purple polyhedral, respectively.

Figure 1 represents the MIL-127 structure which exhibits a 3D microporous system with hydrophilic groups (trimers of iron (III)) and hydrophobic groups (organic linker). The framework topology of each trimers unit are linked by six carboxyl bonds (Fig. 1b). MIL-127(Fe) is a stable framework with large windows/pores and it contains two types of pores, *i.e.* an accessible channel system (~ 6 Å) and a cage of around 10 Å diameter accessible through apertures of channels in x- and y- directions and apertures (also called windows) between cavities. Due to its large pore size, MIL-127(Fe) is expected to be a good candidate for storing or separating various types of small gas molecules.

1.3 Applications

MOF structures provide many interesting characteristics, for instance, large surface area, high porosity, high thermal stability and they can easily be modified by adjustment of metal cluster or organic linkers. [11, 12] From these various properties

of MOFs it follows that they are well suited for potential applications such as gas storage, gas separation, catalysis and biological applications. [13-17]

1.3.1 Gas storage

There are a lot of different approaches that we use to store environmentally gas molecules. MOFs offer a variety of chemical compositions and structural architectures. Furthermore, MOFs having a large surface area and having pore sizes similar or slightly larger to the magnitude of common gas molecules. So, it provide a great possibility for gas adsorption or gas storage applications. [18] It is expected that MIL-127(Fe) could be used for gas storage or adsorption like MIL-100 and MIL-101. [19]

1.3.2 Gas separation

Separation processes play significant roles in chemical industry and daily life. A several porous materials have been examined as the adsorbents or have been applied as membrane filler materials for separations. [11] MOFs provide a one material that can be used in separation process. For example, Castillo *et al.* [20] have reported the separation performance of MIL-47 for xylene isomers.

1.3.3 Catalysis

One important property of MOFs is heterogeneous catalysts. Due to their higher surface area and having a large pore size, an active species can be encapsulated into the pores of MOFs. MOFs can act as the host for metal nanoparticles by acting as Lewis acid or redox center. A variety of MOFs have been reported as a catalysts. [21-23] Interestingly, MIL-127(Fe) has been reported for the catalytic activity as solid Lewis acids for the isomerization. [24]

1.4 Literature reviews

Since MIL-127(Fe) are reported as a new type of porous material. There are a few research that mention about MIL-127(Fe). Almost all publications that investigated MIL-127 have been experimental studies.

In 2007, Liu *et al.* [25] reported structures of MOFs which based on indium trimer building blocks. The trimers of octahedral sharing one central μ_3 – oxo anion to form trimeric building blocks. This structure consists of two components; indium trimer building block and 3,3',5,5'-azobenzenetetracarboxylic acid. The 3D network having square octahedral topology, so we called *soc*-MOF(In). From the structural analysis combined with inelastic neutron scattering (INS) and sorption study, they found that the structure of *soc*-MOF(In) is suitable for high hydrogen storage. The model of *soc*-MOF(In) was used as a template for MIL-127(Fe).

In 2012, Dhakshinamoorthy *et al.* [24] have developed MIL-127(Fe) or *soc*-MOF(Fe) as a heterogeneous catalyst for the rearrangement of α -pinene oxide. The structure of MIL-127(Fe) has been shown to be analogue to *soc*-MOF(In). They reported the formula of MIL-127(Fe) or *soc*-MOF(Fe) as $\text{Fe}_3\text{O}(\text{Tazb})_{4/3}\text{X}$ (X = OH,Cl). The catalytic properties of MIL-127(Fe) have been tested for this rearrangement reaction in the absence of solvent. MIL-127(Fe) is the material containing iron metal sites which acts as Lewis acid. In addition, they reported the BET surface area ($S_{\text{BET}} \sim 1400 \text{ m}^2\text{g}^{-1}$) and pore dimension to be around 10 Å.

In 2013, Cunha *et al.* [26] studied drug encapsulation and release kinetic of caffeine in MIL-127(Fe) to get deeper understanding of the encapsulation of drug by MOFs with different topologies and compositions. In addition, they reported the cubic structure of *soc*-MOF(Fe) or MIL-127(Fe) to be consisted of two types of pores: the cage (~ 10 Å) and the 1D channel (~ 6 Å). For 1D channel, it was assumed that the accessibility of the windows will be through narrow apertures of ~ 4 Å. Due to the appropriate pore size, so it is possible for adsorption of small gases molecules in this material.

In 2014, Eubank *et al.* [27] have investigated sorption properties the biological gas nitric oxide (NO) on porous rigid MIL-127(Fe) experimentally. They reported not only the NO sorption properties but also release properties of porous materials: MIL-

100(Fe, Cr) and MIL-127(Fe). For MIL-127(Fe), they reported that the Lewis acid sites are able to adsorb a few of nitric oxide at 298 K.

In 2015, Wongsakulphasatch *et al.* [28] have reported the scalable preparation of mixed metal Fe(III)/M(II) (M = Co, Ni, Mg) porous materials with control iron/metal stoichiometry. IR spectroscopy including adsorption studies of MIL-127(Fe) were reported. The carbon monoxide and carbon dioxide sorption in both MIL-127(Fe) and mixed iron (III) metal of MIL-127 are obtained in term of adsorption isotherm at 303 K. The adsorption isotherm results from this experimental study were compared with our simulations.

Recently, Chevreau *et al.* [29] have reported the new strategies for controlled-size synthesis, scale up and full characterization of MIL-127(Fe). They showed how to synthesize MIL-127(Fe) with low-cost and environmentally friendly condition which allows to control crystal size and large-scale production.

1.5 Scope of this research

The Gibbs Ensemble Monte Carlo (GEMC) simulations with rigid lattice were performed in order to gain insights into the adsorption behaviors of carbon dioxide and carbon monoxide in MIL-127(Fe). Some of force field parameters were taken from different literatures including quantum calculations to obtain the adsorption isotherm from simulations. The results were compared with the experimental results to find the most suitable force field parameters for both MIL-127(Fe) and gases. The Radial Distribution Functions (RDFs), the probability density and the site of the lowest potential energy were determined to locate the preferential adsorption sites of small gases in MIL-127(Fe). Finally, using the most suitable force field parameters, MD simulations were carried out to study the structural and dynamical properties of small gases in this porous material.

CHAPTER II

THEORY BACKGROUND

2.1 Quantum Mechanics

The Quantum mechanics (QM) have been developed over a century to explain microscopic phenomena. The principle of quantum mechanics was begun during the early twentieth century. The theory is formulated in specially developed mathematical formalisms. The limitation of classical mechanic becomes development of the quantum mechanics theory. Quantum mechanics extends classical mechanics ideas to understand the behaviors of subatomic, atomic, molecular species and electronic properties of heavy atoms. [30]

2.1.1 Schrödinger equation

Schrödinger equation is a partial differential equation that describes how the quantum state of a quantum system changes with time. [31] If a particle has wave properties according to de Broglie so it could be described by the combination of the de Broglie and the classical wave equation. Eq. 1 is the time-independent Schrödinger equation for one-dimensional motion. [32]

$$\frac{d^2\Psi}{dx^2} + \frac{8\pi^2m}{h^2}(E - V)\Psi = 0 \quad \text{Eq. 1}$$

where Ψ is the amplitude of the particle/wave at a position x or wave-function, m is the mass of the particle, h is the Planck's constant, E is the energy (kinetic + potential) of the particle and, V is the potential energy of the particle.

The Schrödinger equation plays the role of Newton's laws and conservation of energy in classical mechanics to describe the behavior of a quantum system in terms of wave-function which could be used to elucidate the probability of events or outcome. The combination of kinetic and potential operators so called the

Hamiltonian operator which acts upon the wave-function to generate the evolution of the wave-function in time and space. The Schrödinger equation gives the quantized energies of the system and the form of the wave-function so that other properties may be calculated. However, the Schrödinger equation of atoms or atomic ions with more than one electron could not be solved analytically, because of the mathematical difficulty posed by the Coulomb interaction between the electrons. Hence, it can be solved in exact only for one electron systems like hydrogen atom and hydrogen-like ions (He^+ , Li^{2+} , Be^{3+} and B^{4+})

The general forms of the Schrödinger equation are time-dependent Schrödinger equation and time-independent Schrödinger equation. The time-dependent Schrödinger equation is used to find the wave-function which depends on time following Eq. 2. While the time-independent Schrödinger equation is used to find the wave-function from the stationary states or standing waves following Eq. 3.

$$\hat{H}\Psi(x, t) = i\hbar \frac{\partial}{\partial t} \Psi(x, t) \quad \text{Eq. 2}$$

$$\hat{H}\Psi = E\Psi \quad \text{Eq. 3}$$

\hat{H} is the Hamiltonian operator, Ψ is the wave-function of the quantum system, E is the energy of state, i is the imaginary unit, \hbar is the Planck's constant divided by 2π , and the symbol $\frac{\partial}{\partial t}$ indicates a partial derivative with respect to time, x and t are the position vector and time respectively.

2.1.2 Born-Oppenheimer approximation

The Born-Oppenheimer (BO) approximation is the assumption that the motion of nuclei and electrons can be separated due to the fact that the mass of nucleus is around 1,800 times heavier than that of electron. The nuclei move very slowly when compared with the movement of electrons. Thus, the nuclear positions are seemingly fixed with respect to the electronic motion. The nonrelativistic Hamiltonian for a molecule could be shown in Eq. 4 or in more compactly form in Eq. 5. [33]

$$\hat{H} = -\frac{1}{2} \sum_i \nabla_i^2 - \sum_A \frac{1}{2M_A} \nabla_A^2 - \sum_{A,i} \frac{Z_A}{r_{Ai}} + \sum_{A>B} \frac{Z_A Z_B}{R_{AB}} + \sum_{i>j} \frac{1}{r_{ij}} \quad \text{Eq. 4}$$

$$\hat{H} = \hat{T}_e(r) + \hat{T}_N(R) + \hat{V}_{eN}(r, R) + \hat{V}_{NN}(R) + \hat{V}_{ee}(r) \quad \text{Eq. 5}$$

where i, j refer to electrons, A, B refer to nucleus, Z is the nuclear charge, M_A is the proportion of mass of nucleus A to the mass of electron, R_{AB} is the distance between nuclei A and B , r_{Ai} is the distance between nucleus A and electron i , r_{ij} is the distance between electron i and j . \hat{T}_e, \hat{T}_N refer to the kinetic energy terms of electrons and nucleus and \hat{V} refers to the Coulomb terms.

Substituting Eq. 5 to the Schrödinger equation, one obtains

$$(\hat{T}_N + \hat{T}_e + \hat{V}_{ee} + \hat{V}_{eN} + \hat{V}_{NN}) \Psi(r; R) = E \Psi(r; R) \quad \text{Eq. 6}$$

Imposing the Born-Oppenheimer approximation, the solutions for nuclei and electrons can be separated, and

$$\Psi(r; R) = \Psi_{nu}(R) \Psi_{el}(r; R) \quad \text{Eq. 7}$$

where Ψ_{nu}, Ψ_{el} = nuclear, electronic wave-function. The former depends on only nuclear coordinates and the latter depends on electronic coordinates at fixed nuclei R .

At fixed nuclei configuration, the term $\sum_A \frac{1}{2M_A} \nabla_A^2$ is expected to be small and $\sum_{A>B} \frac{Z_A Z_B}{R_{AB}}$ is a constant. So they can be neglected. So that. Thus, Eq. 6 becomes

$$[\hat{T}_e(r) + \hat{V}_{eN}(r, R) + \hat{V}_{ee}(r)] \Psi_{el}(r) = E_{el} \Psi_{el}(r) \quad \text{Eq. 8}$$

$$\left[-\frac{1}{2} \sum_i \nabla_i^2 - \sum_{A,i} \frac{Z_A}{r_{Ai}} + \sum_{i>j} \frac{1}{r_{ij}} \right] \Psi_{el} = E_{el} \Psi_{el} \quad \text{Eq. 9}$$

or
$$\hat{H}_{el} \Psi_{el} = E_{el} \Psi_{el} \quad \text{Eq. 10}$$

Hence, the solution of molecular Schrödinger equation can be obtained by just solving the electronic Schrödinger equation. The $E_{el} + \hat{V}_{NN}$ is the potential energy and it governs all chemical properties.

2.1.3 Hartree-Fock method

Hartree-Fock (HF) method is a method for approximately solving the electronic Schrödinger equation which is similarly to the molecular orbital approximation. [34] The approximation avoids electron-electron interactions and considers each electron to move in electrostatic field of their neighbors. The wave-function of the system is approximated by the single Slater determinant and the solution is obtained by the variation principle. The new operator including Coulomb and exchange operator was introduced as Fock operator which shows in Eq. 11 and finally, the Hartree-Fock equations are shown in Eq. 12.

$$f(x_1) = h(x_1) + \sum_j J_j(x_1) - K_j(x_1) \quad \text{Eq. 11}$$

$$f(x_1)\chi_i(x_1) = \varepsilon_i\chi_i(x_1) \quad \text{Eq. 12}$$

where $J_j(x_1)$ is Coulomb operator, $K_j(x_1)$ is an exchange operator, ε_i is the energy eigenvalue associated with orbital χ_i .

The HF equation is non-linear. Thus, we can determine the set of orbitals by the self-consistent field (SCF) approach. [35]

2.1.4 Basis sets

The Basis set is a set of known mathematical functions. In quantum chemical calculations, the linear combination of atomic orbital (LCAO) is normally used to construct the molecular orbital (MO). The atomic orbital represents one electron wave-function and it can be written in terms of the summation of the basis functions, Eq. 13, where $c_{\mu i}$ is the orbital coefficients. The basis functions can be described by

either Slater-type orbitals (STOs) or Gaussian-type orbitals (GTOs) [36]. Forms of STOs and GTOs were given in Eq. 14 and Eq. 15

$$\phi_i = \sum_{\mu=1}^N c_{\mu i} \chi_{\mu} \quad \text{Eq. 13}$$

$$\chi_{n,l,m}(r, \theta, \phi) = N_{n,l,m} Y_{l,m}(\theta, \phi) r^{n-1} e^{-\zeta r} \quad \text{Eq. 14}$$

$$\chi_{a,b,c}(r, \theta, \phi) = N_{a,b,c,\alpha} x^a y^b z^c e^{-\alpha r^2} \quad \text{Eq. 15}$$

where x, y, z are Cartesian coordinate, N is a normalizing constant, a, b, c are natural number, n, l, m are angular momentum quantum number, r is the distance of the electron from nucleus and ζ is a constant related to the effective charge of the nucleus and $e^{-\alpha r^2}$ is a Gaussian functions.

The STOs basis function is the analytical stationary Schrödinger equation for one electron atom. In order to perform SCF calculations, the four-center two-electron integrals must be computed. For STOs, the calculation of the four-center two-electron integral takes very long time. While it is much more faster when computes using GTOs, although more integrals are required. Therefore, GTOs are more widely used than STOs.

There are several classes of basis set which are classified by type and number of functions being include. They are:

1) Minimal basis set

This basis set required only one basis function for each atomic orbital also known as a single zeta basis set. The common minimal basis set is STO-nG, where n being the number of primitive Gaussian functions. A STO-3G basis set is commonly used.

2) Extended basis set

The extended basis set is the basis set with more than one basis function per atomic orbital. There are several types of extended basis sets which are:

Multiple zeta basis set

For this basis set, the valence orbital is split into inner and outer function so called the split valence basis set. The inner function has larger ζ exponent which means the atomic orbital is more contracted. The outer function has smaller ζ exponent which means the atomic orbital is more diffuse. The most commonly used basis functions are 3-21G and 6-31G.

Polarized basis set

In polarized basis set, polarization functions which are functions with higher angular momentum are added to the split-valence basis set. The addition of higher angular momentum functions will give flexibility or can allow orbitals to become polarized. In principal, s-orbital can polarize if mixed with p-orbitals and p-orbitals can polarize if mixed with d-orbitals. To polarize a basis function with angular momentum (ℓ), it should be mixed with another basis function with angular momentum ($\ell + 1$).

Diffuse basis set

In diffuse basis set, diffuse functions which are additional functions with very small exponents are added to extended basis set. The addition of the diffuse function allows diffusive electron behavior. Diffuse basis sets are necessary for correct description of anions and weak bonds and they are frequently used for calculations of properties such as dipole moments, polarizability, etc.

2.2 Simulations

In quantum mechanical calculations, the properties of static quantum system can be obtained. In order to understand the dynamic properties, a common way is using the statistical mechanics. A statistical mechanics is theoretical studied of the thermodynamic behavior of large system by apply probability theory. Statistical mechanics provides a framework for relating the microscopic properties of individual atoms and molecules to the macroscopic bulk properties of materials that can be

observed in everyday life. Statistical mechanics introduces the statistical ensemble in order to define thermodynamic properties of the systems.

2.2.1 Ensemble

An ensemble was a collection of imaginary replication of the thermodynamic systems. [37] All possible systems differ in microscopic states but have an identical macroscopic or thermodynamic state. Each thermodynamic system represents a possible state that can be occurred in the real system. In general, the pressure (P), volume (V), temperature (T) and number of molecules (N) were defined as thermodynamic state. The different three general approaches which important in statistical thermodynamics consist of

1) Microcanonical ensemble or NVE ensemble

A microcanonical ensemble is the statistical ensemble which represents the possible states in statistical mechanical system with certain total energy. The system cannot exchange the energy or particles with environments. The thermodynamic state is determined by fixing number of particle in the system (N), volume (V) and total energy (E).

2) Canonical ensemble or NVT ensemble

A canonical ensemble is the statistical ensemble which represents the possible states in statistical mechanical system in thermal equilibrium with heat bath. The energy of the system can exchange with the heat bath and the different between each states can be found in the total energy. The thermodynamic state is determined by fixing number of particle in the system (N), volume (V) and temperature (T).

3) Grand canonical ensemble or μVT ensemble

A grandcanonical ensemble is the statistical ensemble which represents the possible states in statistical mechanical system in thermodynamic equilibrium with reservoir (surroundings). The system can exchange both energy and particles with

reservoir. The thermodynamic state is determined by chemical potential (μ), volume (V) and temperature (T).

The ensembles are criteria that we choose to determine the system, before performing the simulations, the energy of the system must be evaluated by using quantum mechanics. However, the energetic calculation by quantum mechanics are not practically in a large system. The alternative way is using molecular mechanics.

2.2.2 Molecular mechanics and Force Field parameters

The basic functional form and parameter sets which used to described the potential energy of the system in molecular simulations. The total energy can be written in Eq. 16 which depend on bonded potential and nonbonded potential.

$$E_{total} = E_{bonded} + E_{nonbonded} \quad \text{Eq. 16}$$

The bonded potential or intramolecular potential can be described by bonds stretching, angle bending and dihedral angle torsion as shown in figure 2.

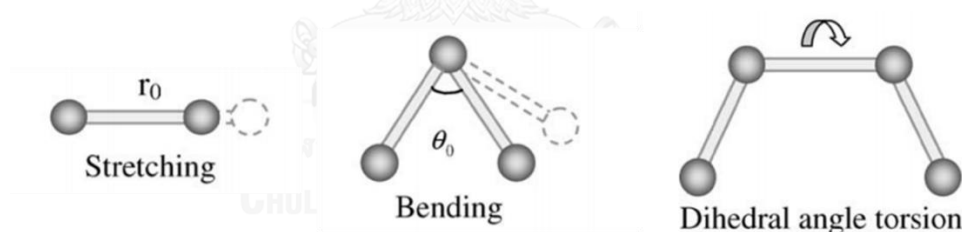


Figure 2 The interatomic interactions in molecular mechanics [38]

The potential energy can be found from the summation of bond potentials, angle potential and dihedrals potential which shown in Eq. 17.

$$E_{bonded} = \sum_{bonds} K_b (r - r_0)^2 + \sum_{angles} K_\theta (\theta - \theta_0)^2 + \sum_{dihedrals} K_\phi [1 + \cos(n\phi - \phi_0)] \quad \text{Eq. 17}$$

where K_b , K_θ , K_ϕ are the force constant of the bond stretching, angle bending and dihedral angle constant. r_0 , θ_0 , ϕ_0 are the equilibrium bond distance, equilibrium angle and equilibrium dihedral angle.

For nonbonded potential or intermolecular potential, the potential energy is based on the Van Der Waals potential and electrostatic or Coulomb potential following Eq. 18.

$$E_{nonbonded} = E_{Electrostatic} + E_{Van Der Waals} = \sum_{i<j} \frac{q_i q_j}{4\pi\epsilon_0 r_{ij}} + \sum_{i<j} 4\epsilon_{ij} \left[\left(\frac{\sigma_{ij}}{r_{ij}} \right)^{12} - \left(\frac{\sigma_{ij}}{r_{ij}} \right)^6 \right] \text{ Eq. 18}$$

where q_i, q_j are the atomic charges of atom i and j , ϵ_0 is the effective dielectric constant, r_{ij} is the distance between atom i and j , ϵ_{ij} is the potential well depth and σ_{ij} is the distance between atom i and j at the zero potential energy

For the Van Der Waals potential, it can be described by the attractive forces and repulsive forces in term of Lennard-Jones potential which displayed in figure 3.

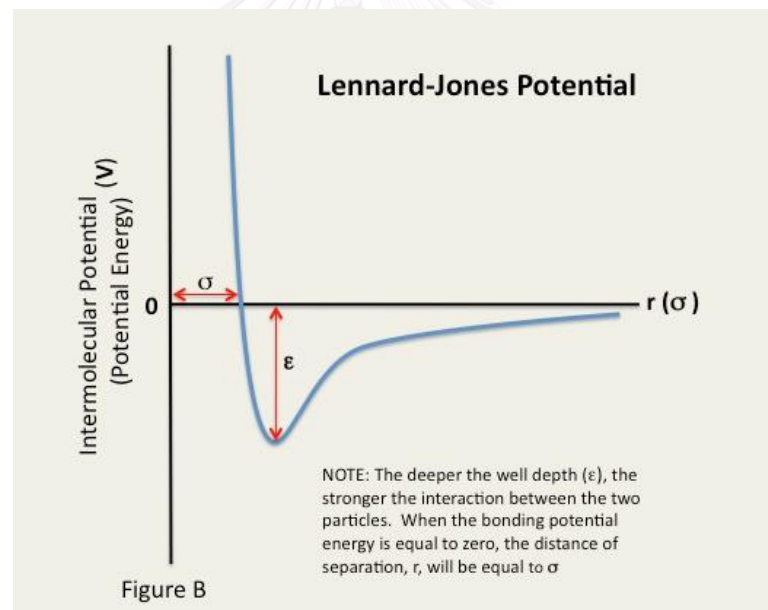


Figure 3 The Lennard-Jones potential use to describe interatomic potential of molecule. [39]

For the electrostatic potential, Interactions between molecules due to their permanent dipole moments are described approximately by treating the charged portions of the molecule as point charges. Herein, The Coulomb potential is the effective pair potential which used to describe the interaction between two point

charges. The Coulomb potential for point charges were used to estimate the forces between the charged portions of each molecule and the charged parts of neighboring molecule.

For unlike Lennard-Jones interactions, the Lorentz-Berthelot combining rules were applied following Eq. 19 for diatomic parameters.

$$\sigma_{ij} = \frac{1}{2}(\sigma_{ii} + \sigma_{jj}) \quad , \quad \epsilon_{ij} = \sqrt{\epsilon_{ii}\epsilon_{jj}} \quad \text{Eq. 19}$$

2.2.3 Monte Carlo (MC) simulations

One approximate approach that is well suited to computers calculation is the Monte Carlo method. Monte Carlo is the mathematical methods that use random numbers for solving quantitative problems. Monte Carlo simulation performs analysis by building models of possible results by a range of probability distribution for any factor that has inherent uncertainty. Then the results were calculated over and over, each time using a different set of random values from the probability functions. The difference of this approach can rely on equilibrium statistical mechanics rather than molecular dynamics.

2.2.3.1 Gibbs ensemble Monte Carlo (GEMC) simulations

The Gibbs ensemble Monte Carlo method have been developed for calculation of coexistence phase in a new ensemble. [40] This technique makes two simulation boxes which are in thermodynamic contact. The particles can swap between two simulation boxes to create chemical potential equilibrium between two phases with no physical contact. [41] The useful of Gibb ensemble Monte Carlo are applied to the calculation of the liquid-vapor coexistence or solid-vapor coexistence. In this work, GEMCs have been applied for the calculation of adsorption isotherm between porous solid material and small gas molecules.

In principle of the GEMCs following figure 4, consider two simulations cell are occurred simultaneously with different phase. The region I is the vapor phase or gas

phase and another one is liquid phase or solid phase. The systems have constant number of particles (N), volume (V) and temperature (T) in the initial conditions. Three types of movement that satisfied for thermodynamics requirement composed of the particles displacement within each region, volume changes of two regions and particle transfer between two regions. These moves were continued until the system get internal equilibrium in equality of pressure and chemical potentials.

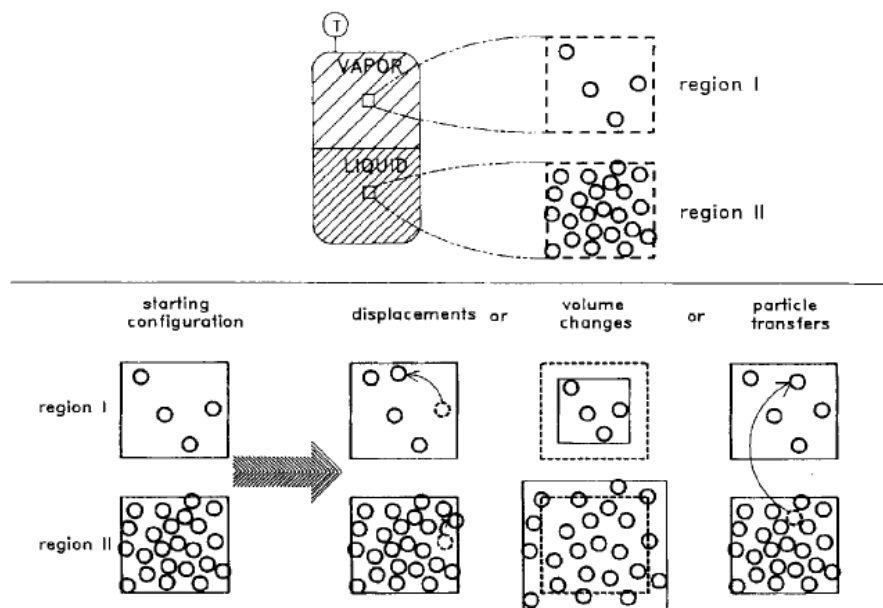


Figure 4 Schematic illustration of movement in Gibbs ensemble Monte Carlo (GEMC) simulations. [42]

2.2.4 Molecular Dynamics (MD) simulations

The molecular dynamics simulation provides time dependent behavior of a molecular system. It can be used to investigate the structure, dynamics and thermodynamic properties of molecules. The principle of MD simulations based on Newton's second law or equations of motion following Eq. 20.

$$F_i = m_i a_i = m_i \left(\frac{d^2 r}{dt^2} \right) \quad \text{Eq. 20}$$

where F_i is the force on particle i , m_i is the mass of particle i , a_i is the particle's acceleration, r is the position and t is a time.

Integration of the equations of motion will be obtained the trajectory which describes the position, velocity and acceleration of particle in a function of time.

2.2.4.1 Integration algorithms

The equations of motion in MD simulations are deterministic. To solve equations of motion, the initial positions of particles, velocities and acceleration are determined by the potential energy function. This function will be solved numerically for all trajectories in MD system. Many of algorithms can be used to integrate the equations of motion such as Verlet algorithm, Leap-frog algorithm, Velocity Verlet algorithm and Beeman's algorithm. The integration algorithms suppose the positions, velocities and accelerations by approximation from a Taylor series expansion. The important criteria for considering the algorithm that will be applied are: computational efficiency and allowing a long time step for integration and conservation of energy and momentum.

In this study, the Verlet algorithm via DL_POLY software is applied for integration of equations of motion. The equations from Verlet algorithm can be written as

$$r(t + \delta t) = 2r(t) - r(t - \delta t) + a(t)\delta t^2 \quad \text{Eq. 21}$$

where r is the position, a is the acceleration (the second derivative with respect to time, t .)

The Verlet algorithm determined only the positions at time t and positions at time $t - \delta t$ to construct new position at time $t + \delta t$. The Verlet algorithm do not have explicit velocities. The advantages of using Verlet algorithm are the straightforward derivation and the simple storage requirements. However, the disadvantage of using this algorithm is the tolerable precision.

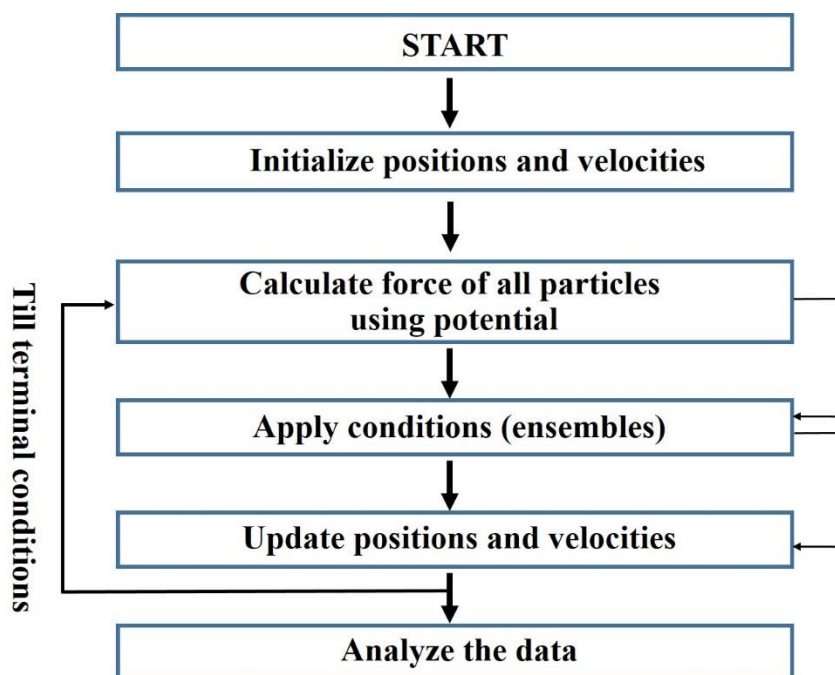


Figure 5 Schematic representation of Molecular dynamics simulation diagram.

The performance of MD simulations can be easily described in figure 5. Firstly, the initial positions and velocities of the particles are constructed and the simulation time steps are set. Then, the positions and velocities of the next stage are predicted by solving the equation of motion. Select ensemble conditions are applied in the next step. Finally, the positions and velocities are updated. These processes are continued until the simulation reaches the final time. The trajectory from MD simulations contains a lot of physical and dynamic properties to analyze.

2.2.5 Periodic Boundary Condition

Periodic boundary conditions (PBC) have been widely used in computational calculation to represent infinite system.

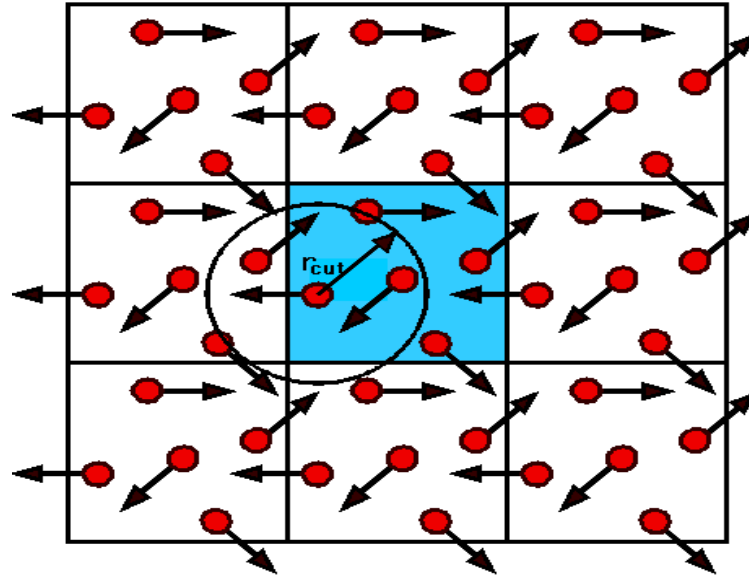


Figure 6 Schematic represent periodic boundary conditions in two dimensions [43]

In the simulations, the primary cell is replicated in all direction as image cells as shown in figure 6. The primary and image cells have similar in number of particles, position of particles, size and shape of simulation boxes. So particles interact not only within one simulation box, but also with another image boxes. Surrounding the box with replication of itself will avoid the problem from surface effect. The minimum image convention is required as a spherical cut-off radius for each atom which interacts with the nearest neighbors in the periodic array. The cut-off will reduce the number of computations. [44]

In general, the cubic box shape is commonly used for the periodic simulation because it is easy to visualize. However, there are another shape of simulation box such as truncated octahedron, hexagonal prism, rhombic dodecahedron, etc.

2.2.6 Radial Distribution Functions (RDFs)

The radial distribution function or pair correlation function, $g(r)$, commonly used to interpret the conditional probability of finding atom at the distance r away from the origin in a spherical shell between r and $r + dr$, figure 7.

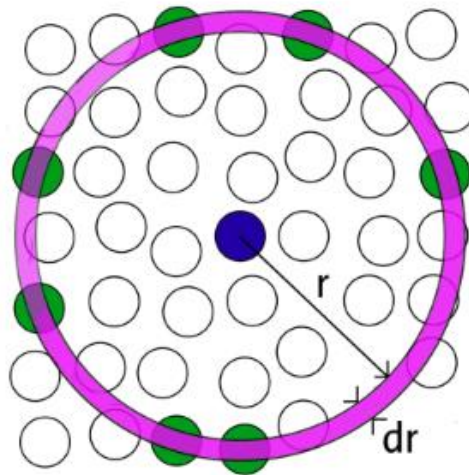


Figure 7 Schematic explanation of the radial distribution functions [45]

The RDF can be expressed as

$$g(r) = \frac{N_{ij}(r + \Delta r)V}{4\pi r^2 \Delta r N_i N_j} \quad \text{Eq. 22}$$

where $g(r)$ is the RDF, r is the distance between atoms i and j , $N_{ij}(r + \Delta r)$ is the number of atom j around i within a shell from r to Δr , V is the system volume, and N_i, N_j are the number of atoms i and j , respectively.

2.2.7 Molecular diffusion

In order to describe the distribution of molecules through random motion. The diffusion of the molecules were used to describe the dynamic behavior [46]

$$\frac{\partial}{\partial t} c(r,t) = D\nabla^2 c(r,t) \quad \text{Eq. 23}$$

$$J = -D\nabla c \quad \text{Eq. 24}$$

where $c(r,t)$ is a function that describes the distribution of probability of finding molecules at position r at time t , D is the diffusion coefficient.

The term c can interpreted as concentration corresponding to Fick's first law (Eq. 24). J is the diffusion flux of the concentration. The mathematical equation can be solved by using Green's function and the position of molecules are measured by the mean square displacement (MSD).

$$\langle [r(t) - r(0)]^2 \rangle = 6Dt \quad \text{Eq. 25}$$

The mean square displacement is a measure of average distance travelled by molecules. This equation used by Einstein in the study of Brownian motion of particles. When the distance of molecules travelled is proportional to time, the self-diffusion coefficient (D_s) is obtained.

CHAPTER III

CALCULATION DETAILS

3.1 Quantum Mechanical calculations

Atomic partial charges are one of the parameters that are required for the simulations. Several methods can be used to calculate the atomic partial charges, for instance, the Mulliken charge [47], the electrostatic potential (ESP) [48], the charges from electrostatic potentials using a grid based method (CHELPG) [49] *etc.* In the present work, the ESP method was chosen for estimating the atomic partial charges. For the ESP method, the electrostatic potential was fitted on a grid which surrounded the molecules. In this work, we separated the structure into two types for calculating the ESP charges as shown in Fig. 8. The calculations were performed by the Gaussian09 program [50] using the Hartree-Fock (HF) method with 6-31G* basis set. Subsequently, the ESP charges from two structures were applied to the force field parameters for the simulations.

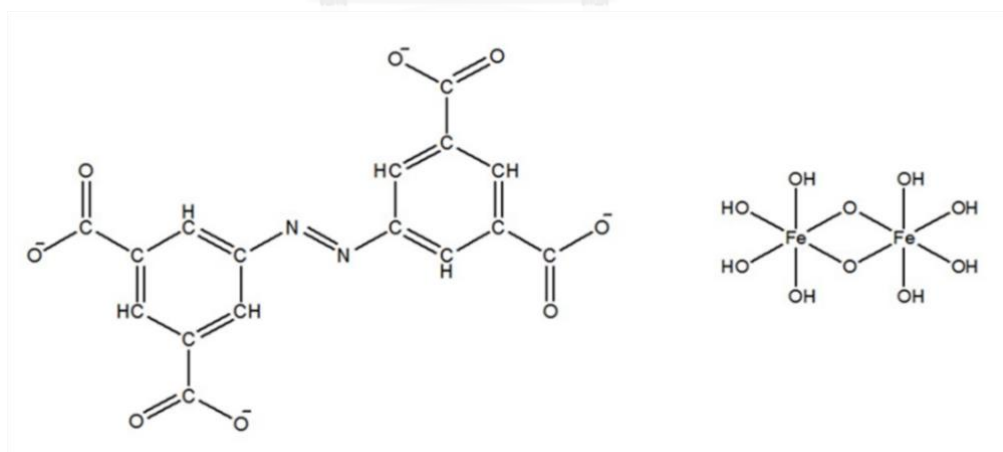


Figure 8 Two structures used to estimate the electrostatic potential (ESP) charges for organic linker (left) and metal cluster (right) in MIL-127(Fe).

3.2 Simulations

The crystal structure of the MIL-127(Fe) was constructed from X-ray diffraction (XRD) data. This is an ideal lattice averaged from experimental data. Consequently, the impurities that exist in the real MIL-127(Fe) will not appear. The structure was generated to consist of 27 (3×3×3) unit cells and 8 (2×2×2) unit cells for using in the GEMC and the MD simulations, respectively. Periodical boundary conditions have been applied in both GEMC and MD to model a virtually infinite system. The force field parameters of a given atom in the lattice are depended upon the surrounding of this atom. Therefore, fictive atom types N_N, C_H, C_O, C_N, C_C, O_O, O_Fe, O_Z, H and Fe have been defined in the MOF structure, respectively. Their positions within the lattice can be seen in Fig. 9.

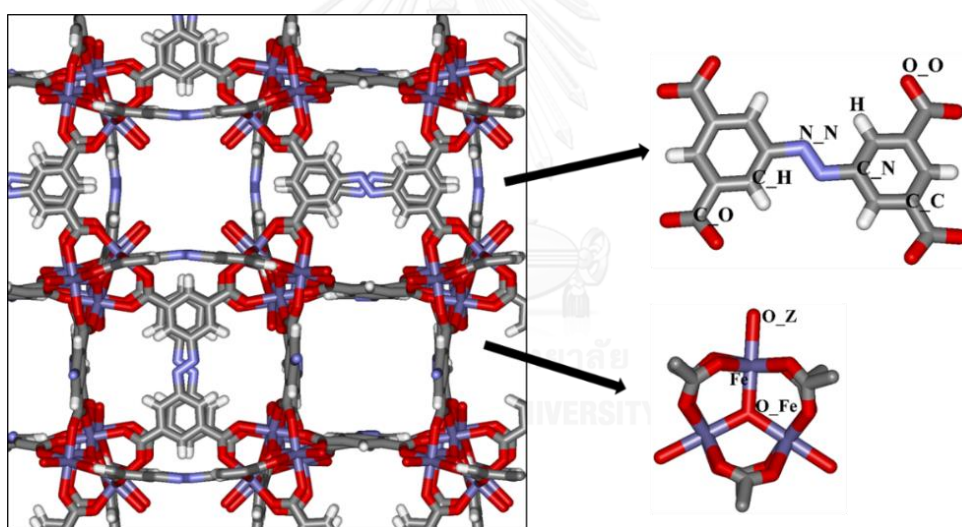


Figure 9 The structure of MIL-127(Fe) as constructed from XRD data composing of metal cluster and organic linker. The carbon, hydrogen, oxygen, nitrogen and iron atoms are shown by grey, white, red, blue and purple colors, respectively. In addition, the label of atom types in the MIL-127(Fe) are displayed.

3.2.1 Force fields

In computational simulations, the force field parameters which describe the potential energy of the systems, are based on bonded and nonbonded interactions.

Because of large cavities, channels and connecting windows in MIL-127(Fe) rigid models appear to be reasonable for both MD and MC of diffusion and adsorption of the small gas molecules. For the rigid MOFs structure, only the nonbonded interactions play a role that can be described by Lennard-Jones (LJ) and Coulombic potentials following the equation 18.

Different LJ parameters of carbon, hydrogen, oxygen and nitrogen atoms were compared. They were taken from Universal Force Field (UFF) [51], DREIDING [52], and the literature from Babarao et al. [53] whereas the parameters of the iron atom were always taken from UFF. The parameter data were shown in Table 1. Atomic charges from QM calculations were adopted to each atom type in the material.

The structure of the carbon dioxide molecule, was modelled as a rigid linear molecule. The LJ parameters including the charges of carbon and oxygen atoms were taken from Potoff and Siepmann (FF1) [54] and Liu *et. al.* (FF2) [55] with the bond length of 1.16 Å. The parameters are shown in Table 2 and Table 3. Furthermore, the five sets of the carbon dioxide charges were prepared following the literature [56-60] for adjustment of the force field parameters.

Table 1 The Lennard-Jones potential parameters for MIL-127(Fe)

Atom types	UFF [51]		DREIDING [52]		Literature [53]	
	σ (Å)	ϵ (kcal/mol)	σ (Å)	ϵ (kcal/mol)	σ (Å)	ϵ (kcal/mol)
N_N	3.660	0.069	3.6621	0.0774	3.261	0.0686
C_O	3.851	0.105	3.8983	0.0951	3.431	0.1045
C_H	3.851	0.105	3.8983	0.0951	3.431	0.1045
C_N	3.851	0.105	3.8983	0.0951	3.431	0.1045
C_C	3.851	0.105	3.8983	0.0951	3.431	0.1045
O_Fe	3.500	0.060	3.4046	0.0957	3.118	0.0597
O_O	3.500	0.060	3.4046	0.0957	3.118	0.0597
O_Z	3.500	0.060	3.4046	0.0957	3.118	0.0597
H	2.886	0.044	3.195	0.0152	2.571	0.0437
Fe	2.912	0.013	-	-	-	-

Table 2 Force field 1 (FF1) of carbon dioxide [54]

Atom types	σ (Å)	ϵ (kcal/mol)	q (e)
C	2.80	0.05360	+0.70
O	3.05	0.15680	-0.35

Table 3 Force field 2 (FF2) of carbon dioxide [55]

Atom types	σ (Å)	ϵ (kcal/mol)	q (e)
C	3.43	0.10459	+0.544
O	3.12	0.05974	-0.272

For the carbon monoxide molecule, the structure was modelled as a rigid molecule. The LJ parameters were taken from Palucha et al (FF1) [61], Stoll et al (FF2) [62], Straub and Karplus (FF3) [63], Sirjoosingh et al (FF4) [64] and Gu et al (FF5) [65] with bond length 1.128 Å. The data were shown in table 4. However, in free carbon monoxide, the negative charge remains at carbon atom whereas the positive charge remains at the oxygen atom and the molecule has a small dipole moment of 0.122 D. [66] These values were applied for adjustment of the force field parameters.

Table 4 Force field parameters for carbon monoxide.

	Atom types	σ (Å)	ϵ (kJ/mol)	q (e)	Ref.
FF1	C	3.55	0.3089	+0.0223	61
	O	2.95	0.5120	-0.0223	
FF2	C	3.7051	0.3068	-0.1347	62
	O	3.7051	0.3068	+0.1347	
FF3	C	4.2990	0.1096	-0.75	63
	X _{com}	-	-	+1.60	
	O	3.5021	0.6657	-0.85	
FF4	C	3.43	0.4409	+0.107	64
	O	3.12	0.2519	-0.107	
FF5	C	-	-	-0.75	65
	X _{com}	4.2238	0.8330	1.60	
	O	-	-	-0.85	

3.2.2 Gibbs ensemble Monte Carlo (GEMC) simulations details

Monte Carlo simulations [40, 67, 68] have been widely used to study the adsorption behavior of guest molecules in MOFs *e.g.* in [4-8, 69]. In the grand canonical Monte Carlo (GCMC) simulation [67, 68], the chemical potential (μ), volume (V) and temperature (T) are fixed. The number of particles and the potential energy are fluctuating according to the Grand Canonical Ensemble. The disadvantage of the GCMC

method is that the pressure or density in a connected free gas phase cannot directly be obtained. Therefore, in order to get directly the value of the gas phase density that is in equilibrium with a given amount of adsorbed molecules, in this work, we performed Gibbs Ensemble Monte Carlo (GEMC) simulations using an in-house software called Gibbon which already used in [6, 8]. In these simulations the system consisted of two simulation boxes. One box contains bulk gas and another one contains the MOF - framework and guest molecules. The temperature of both boxes is equal and it is a fixed input quantity. The Metropolis MC moves were used within each of the two simulation boxes. Additionally the molecules can be swapped between the two boxes in order to ensure equilibrium between them keeping the total number of molecules fixed. The chemical potential can be shown to be equal in both boxes for each sort by the Widom method, but it is not needed for the algorithm. The desired pressure can be chosen by adjustment of the size of the bulk gas box and the total particle number.

In our simulations, the cubic box of the MIL-127(Fe) was fixed at the box length 65.96 Å for GEMC simulations and 43.97 Å for MD simulations. The temperature is fixed at 303 K corresponding to the temperature of the adsorption isotherm from the experiment [28]. In Gibbon, the Coulombic interactions are not calculated by Ewald summation or a similar computer time expensive method. Instead, we use the fact that the sum of Coulombic interactions of the 3 atoms of one complete (in sum neutral) carbon dioxide with the partial charge of a given lattice atom is small for large distances and can be cut off or switched down to zero. The algorithm is described in more detail in [8]. In [70] the method of handling Coulombic charges by collecting charge groups is applied more generally on charge groups in big molecules. The cutoff distance in our GEMC was set as 25 Å for the Coulombic interactions and the LJ interactions. During the simulation, for a given volume of the bulk gas box, the equilibrium between adsorbed molecules and the density in the gas box is obtained. Doing this for different gas phase densities and calculating for each the pressure by the

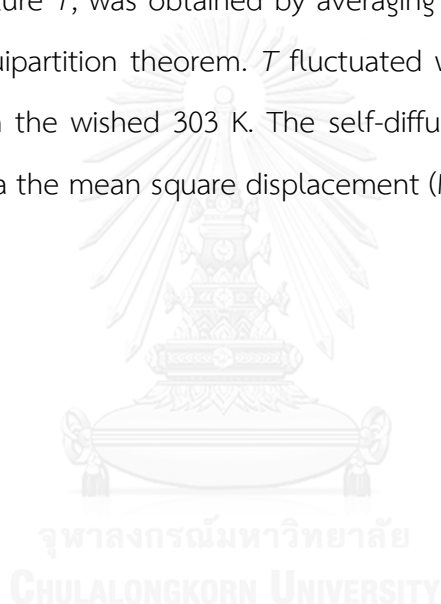
Peng-Robinson equation of state [71] adsorption isotherms are obtained. The first 10^5 steps of the simulation run serve for the relaxation. After an equilibration period of typically 2×10^7 steps, the system in equilibrium was evaluated during another 2×10^7 steps. By using different force field parameters of the MIL-127(Fe), carbon dioxide and carbon monoxide. Adsorption isotherm of carbon dioxide and carbon monoxide in MIL-127(Fe) from GEMC simulations were compared with the experimental data to find the most suitable force field parameters for carbon dioxide and carbon monoxide in MIL-127(Fe). These parameters have then been used to investigate the self-diffusion and the structural properties of the system.

3.2.3 Molecular Dynamics (MD) simulations details

The Molecular Dynamics (MD) simulations [67] were performed using the DL_POLY software [72] to calculate structural and dynamic properties based on Newton's equation of motion. The force field parameters were validated by GEMC simulations, which show good agreement with the experimental results for adsorption for the finally chosen parameter set. The Lorentz-Berthelot mixing rules were applied for the LJ cross parameters. The cutoff distance for the LJ interactions was set to be 18 Å. In this work, we loaded guest molecules in MIL-127(Fe) and simulated in the canonical ensemble (NVT) with Nose-Hoover thermostat for 5 ns to control the temperature at 303 K corresponding to the temperature of the adsorption. The Coulombic fields have been calculated by the Ewald sum because DL_POLY does not provide a charge group algorithm.

In order to learn about the influence of the thermostat on the diffusivity we carried out evaluation runs in both, NVT and in micro-canonical (NVE) ensembles for more than 25 ns to investigate the diffusion of guest molecule in MIL-127(Fe). For the NVE the system was first relaxed and equilibrated for another 0.5 ns before the evaluation started. This comparison NVT/NVE is interesting because on one hand it is known that thermostats can create artefacts (see *e.g.* [73-75]) and they can influence

diffusion results. On the other hand, because of the relatively small number of moving particles in rigid lattice simulation, the question arises if the velocity distribution is really a Boltzmann distribution in NVE. This question was investigated for a similar system by Fritzsche et al. in [76]. In this work it was shown that even for relatively small particle numbers per cage in a rigid zeolite the velocity distribution agreed quite well with a Boltzmann distribution because of the mutual thermalization of the guest molecules. The diffusion coefficients from both ensembles NVT and NVE in the present work are discussed in the results section. The time step in all MD runs was 2 fs. In NVE the average temperature T , was obtained by averaging the fluctuating kinetic energy and applying the equipartition theorem. T fluctuated with an average value of less than 1 per cent from the wished 303 K. The self-diffusion coefficient was obtained from the trajectory via the mean square displacement (MSD) [67].



CHAPTER IV

RESULTS AND DISCUSSION

4.1 Quantum Mechanical calculations

The HF/6-31g* method and ESP approach were used to estimate atomic partial charges of MIL-127(Fe) that we required in the simulations.

Table 5 The adjusted ESP charge of each atom types in MIL-127(Fe).

	Set1	Set2	Set3	Set4
Atom types	q (e)	q (e)	q (e)	q (e)
N_N	-0.171	-0.211	-0.240	-0.260
C_O	0.909	0.750	0.920	0.970
C_H	-0.091	-0.091	-0.120	-0.080
C_N	0.470	0.260	0.400	0.610
C_C	0.082	-0.110	0.090	0.210
O_Fe	-1.131	-1.212	-1.200	-1.050
O_O	-0.788	-0.390	-0.780	-0.800
O_Z	-0.868	-1.012	-0.900	-0.920
H	0.000	0.000	0.000	0.000
Fe	2.389	1.920	2.600	2.000
Total charge	0	0	0	0

The models of the structure for calculation are shown in Fig. 8. Two structures can be used to estimate the charges for metal cluster and organic linker. Some values of the ESP charges have been chosen and made it floating. To avoid artefacts in the Coulombic potential, the charges were adjusted so that the total charge in MIL-127(Fe) is zero. In this work, we examined four sets of charges as shown in Table 5.

4.2 Carbon dioxide in MIL-127

4.2.1 Adsorption isotherms

Gibbs Ensemble Monte Carlo (GEMC) simulations have been employed to find the adsorption isotherms of carbon dioxide in MIL-127(Fe) for different parameter sets in order to find parameters that yield agreement with the experiment. Firstly, the Universal Force Field (UFF) parameters were applied for the Lennard-Jones potential terms for the lattice atoms of MIL-127(Fe) and the charge set 1 from QM was used for the Coulombic potential term. For carbon dioxide, force field parameters adopted from Potoff and Siepmann (FF1) and Liu *et. al.* (FF2) were used. FF1 and FF2 differ in the ϵ value, the value of carbon is smaller than that of oxygen in FF1 and vice versa in FF2, see Table 2 and Table 3. The adsorption isotherm of carbon dioxide in MIL-127(Fe) obtained from the simulations with FF1 and FF2 force field and charge set 1 in comparison with the experiment is given in Fig. 10a. The corresponding adsorption isotherm results for charge set 2 to set 4 are worse.

Table 6 Force Field parameters for MIL-127 and CO₂

MIL-127(Fe)		CO ₂
LJ potential	Coulombic potential	Force Field
UFF	Charge set 1	FF1
DREIDING	Charge set 2	FF2
Literature [53]	Charge set 3	
	Charge set 4	

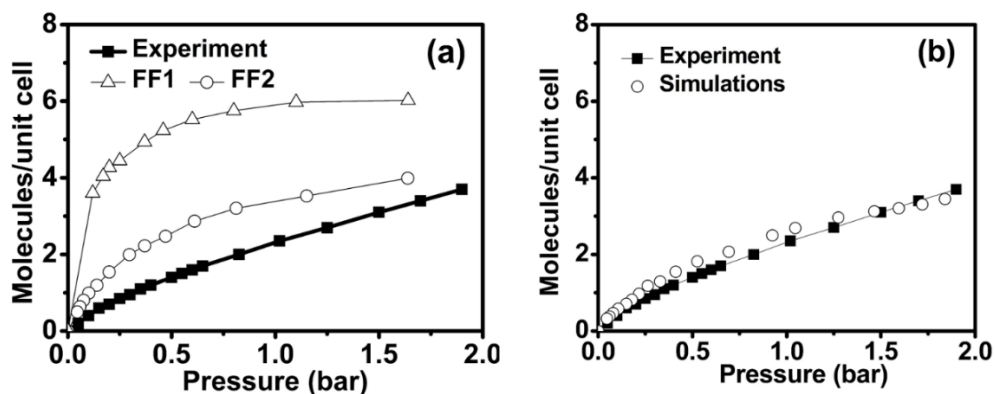


Figure 10 Adsorption isotherms of carbon dioxide in MIL-127(Fe) compared with experimental results using UFF for MIL-127(Fe) and FF1 and FF2 for carbon dioxide (a) and using LJ parameters from Babarao *et. al.* [53] for MIL-127(Fe) and FF2 for carbon dioxide (b)

The isotherm obtained by using FF1 seems to be highly overestimated as compared to the experimental results. Although the isotherm obtained by using FF2 shows better agreement, there remains a large deviation. Thus, the FF2 force field is still suitable for this system. To find the suitable force field for the simulation of carbon dioxide in MIL-127(Fe) we further adjusted atomic charges of carbon dioxide and MIL-127(Fe). The currently applied charge set 1 for the lattice worked reasonably and was maintained. After trying many adjustments, we finally found the best agreement by employing LJ parameters used by Babarao *et. al.* [53] for MIL-127(Fe). The result is displayed in Fig. 10b. The adsorption isotherm obtained from the simulation using these parameters shows the best fit with the experimental result. With this force field, the radial distribution function (RDF) was analysed. This force field was also employed for the MD simulations.

4.2.2 Radial Distribution Functions (RDF)

The Radial Distribution Functions (RDF) obtained from GEMC simulations of carbon dioxide in MIL-127(Fe) were analysed to locate the preferential adsorption sites of carbon dioxide.

Among the many atom types in MIL-127, only atom types which produce dominant peaks are discussed here. Fig. 11 shows RDF's between the carbon dioxide and 3 atom types in MIL-127(Fe), O_Z, O_Fe, and C_N, at three pressures: 0.14, 1.04, and 1.71 bar. Atomic positions of these three atoms were also depicted in Fig. 9.

RDF's for O_Fe, O_Z, and C_N were represented by open circle, open triangle, and filled square symbols in the plots, respectively. The highest peak for O_Fe appears at around 7 Å for all pressures and carbon dioxide atom types, which is the largest distance in comparison to other atoms. This means that carbon dioxide has the weakest affinity to O_Fe. For C_N, RDFs of carbon and oxygen of carbon dioxide show two major peaks around 4 and 6 Å. However, the probability of finding oxygen of carbon dioxide at these two positions is similar while it is more preferable to find carbon of carbon dioxide at 4 Å position except at low pressure. RDFs of carbon and oxygen of carbon dioxide and O_Z appear at the shortest distance, around 3 Å, and there is only one single major peak. The conclusion is that carbon dioxide prefers to adsorb at O_Z position in agreement with Babarao *et. al.* [53] who observed the metal clusters as the preferential adsorption site for IRMOF1. We also observed that only for this position the peak height becomes lower as the pressure increases. This suggests that at higher pressure carbon dioxide can reside at other adsorbed sites. From distances between oxygen and carbon peaks of carbon dioxide and MIL-127(Fe), it can be deduced that carbon of carbon dioxide is preferentially located close to the oxygen atom while oxygen of carbon dioxide is preferentially located close to the oxygen atom of the framework.

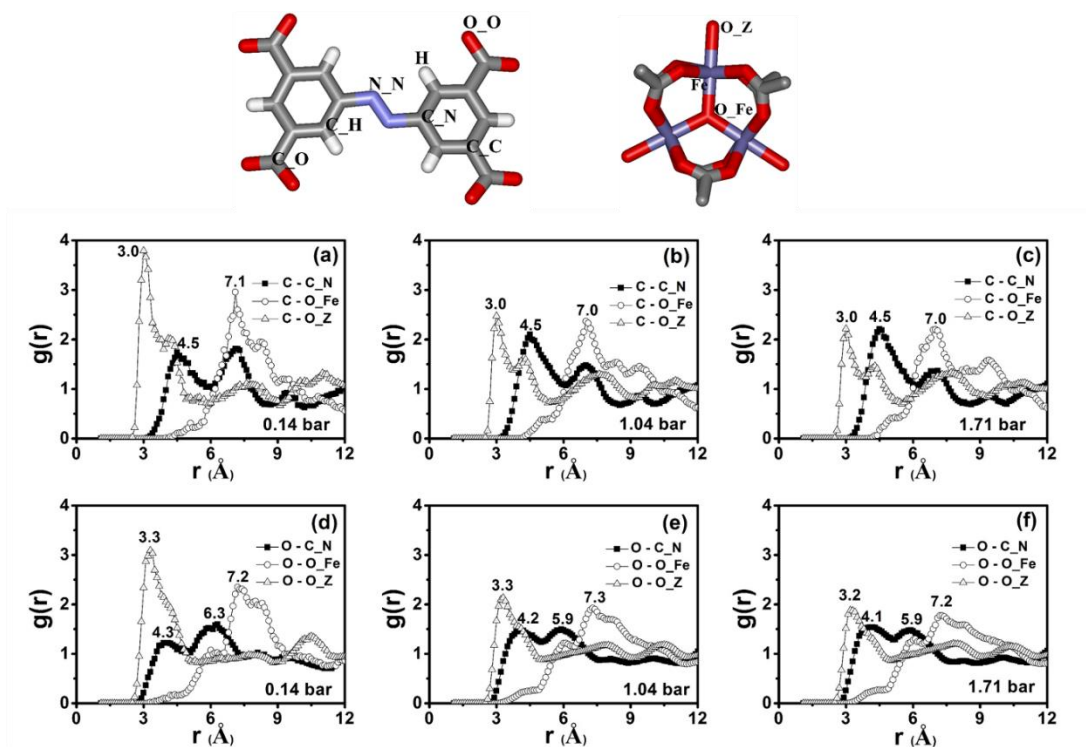


Figure 11 RDF's between carbon of carbon dioxide and 3 atom types in MIL-127(Fe) (a, b, c) and RDF between oxygen of carbon dioxide and 3 atom types in MIL-127(Fe) (d, e, f) at 0.14, 1.04, and 1.71 bar. All graphs were obtained from GEMC simulations.

Since also MD simulations were performed, RDFs obtained from MD and GEMC simulations are compared. As shown in Fig 12 and Fig. 13, a similar pattern was observed for the RDFs obtained from both simulations.

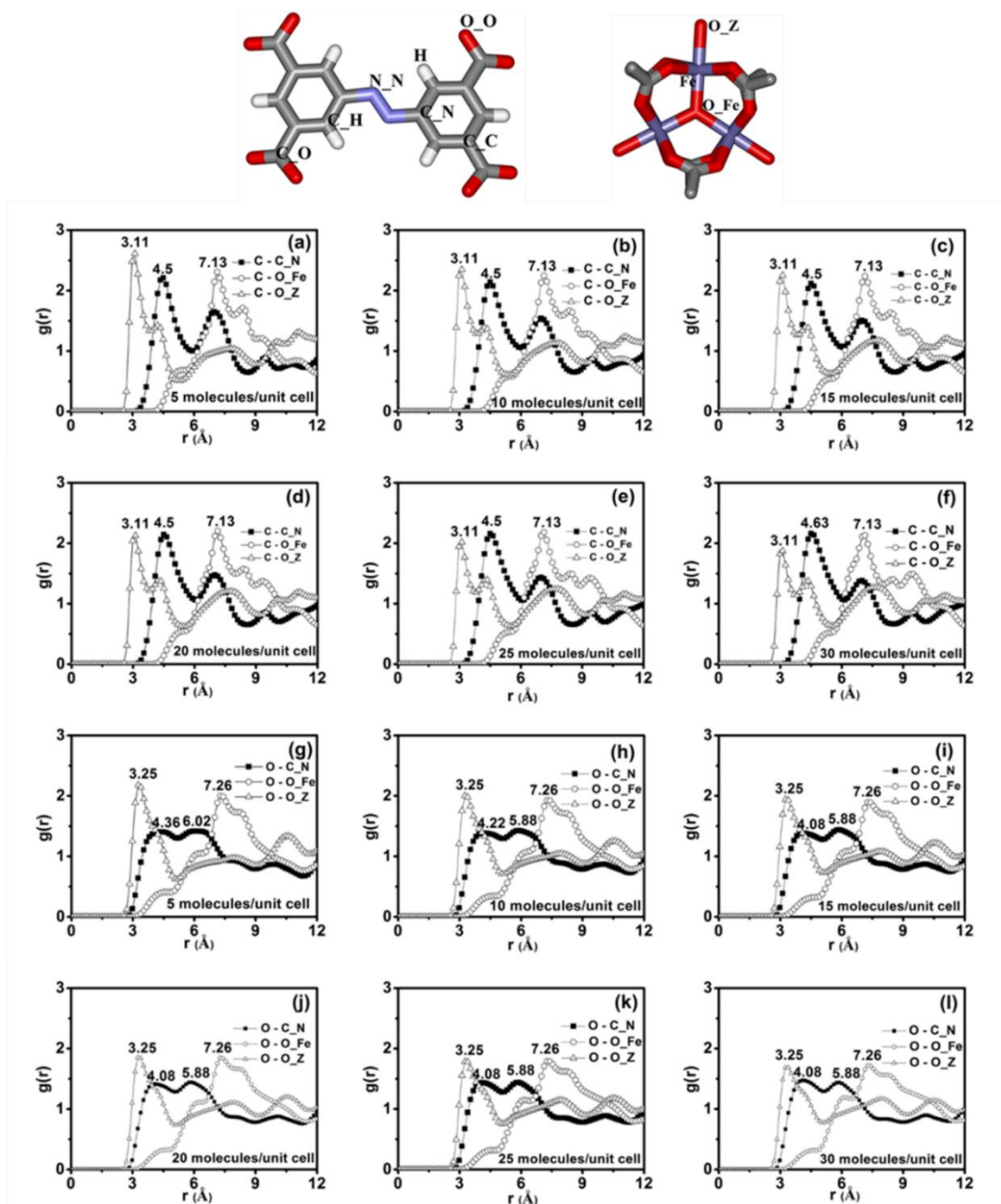


Figure 12 RDF between carbon of carbon dioxide and MIL-127(Fe) (a-f) RDF between oxygen of carbon dioxide and MIL-127(Fe) (g-l) at concentration 5, 10, 15, 20, 25 and 30 molecules/unit cell, respectively. All graphs obtained from MD simulations.

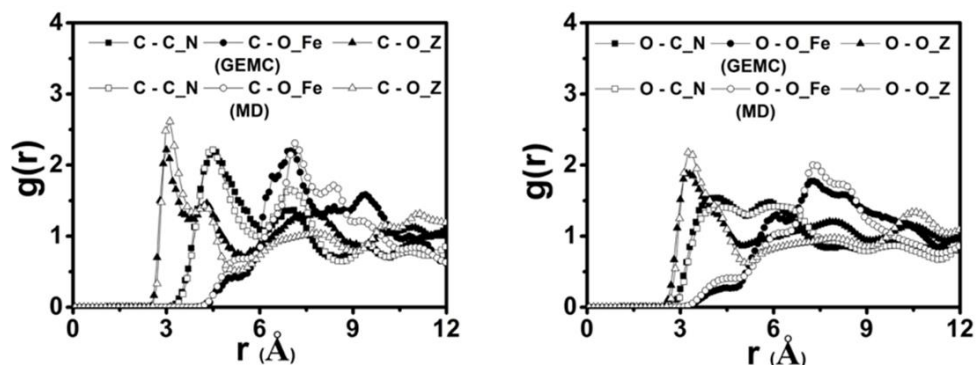


Figure 13 A comparison of RDF between GEMC and MD simulations. The figure on the left side show RDF between carbon of carbon dioxide and 3 atom types in MIL-127(Fe) whereas the figure on the right side show RDF between oxygen of carbon dioxide and 3 atom types in MIL-127(Fe). GEMC data and MD data were obtained at the concentration around 5 molecule/unit cell.

4.2.3 Probability density

Additionally, the probability densities were used to illustrate the adsorption site and the results support the RDF data. Fig. 14 shows the probability density of carbon dioxide inside MIL-127(Fe) in form of clouds of purple dots obtained from GEMC simulations. They are produced by superposition of snapshots of the projection of all positions of the centers of mass of the carbon dioxide molecules onto the xy – plane. Snapshots of simulations were collected every 100000 steps at all pressures.

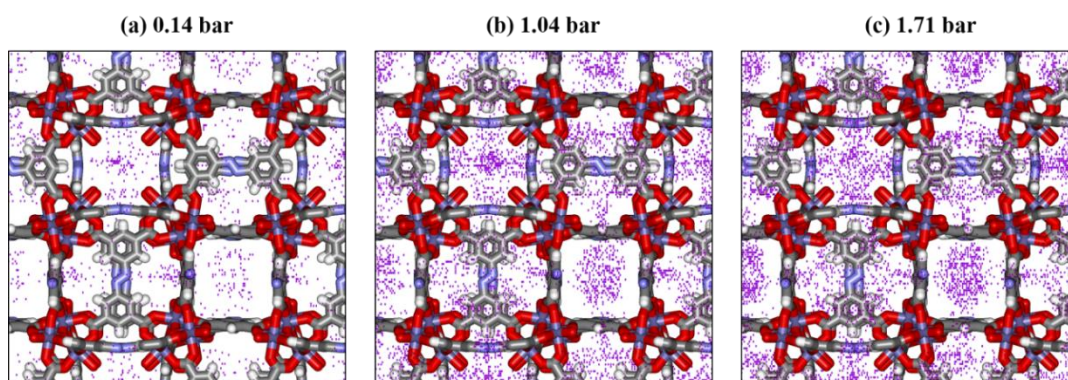


Figure 14 Probability density of carbon dioxide in MIL-127(Fe) obtained from GEMC simulations at pressure (a) 0.14 bar (b) 1.04 bar and (c) 1.71 bar, respectively.

Fig. 14a-c indicates the increase of the density of carbon dioxide as pressure increases in correspondence with the adsorption isotherm. Furthermore, the density plot shows that carbon dioxide molecules spread around the channel of framework. None of carbon dioxide molecules stay inside metal cluster but preferred to adsorb around the metal cluster at all pressures. These results are confirmed by the RDFs which tell us the preferential adsorption site of MIL-127(Fe). At higher pressure, there are many carbon dioxide molecules inside the framework. Thus, carbon dioxide molecules can spread all over the framework but most intensely around the metal clusters. Moreover, we can see the close packing of carbon dioxide molecules which means carbon dioxide molecules can diffuse at high concentration less than at lower concentration because of mutual hindrance. This is in agreement with the diffusion coefficient discussed in section 4.2.5.

4.2.4 Site of the lowest potential energy

As an additional information Fig. 15 shows snapshots of a carbon dioxide molecule at the site and with the orientation of the lowest potential energy found for a carbon dioxide molecule throughout the whole GEMC simulations at the pressure: 0.14, 1.04 and 1.71 bar, respectively. The energies of the carbon dioxide that belong to lowest potential energy are -34.197, -34.211 and -34.257 kJ/mol, respectively. Fig. 15 shows that the carbon dioxide molecule has lowest potential energy near the O_Z position in MIL-127(Fe). This fits well to the RDF results in Fig. 11a which show that the peak of the RDF between carbon of carbon dioxide and O_Z is at about 3.0 Å whereas Fig. 11d shows that the peak between oxygen of carbon dioxide and O_Z is at about 3.3 Å. Accordingly, the distance of the carbon atom is closer to the O_Z position than the oxygen atoms. At the other pressures, the results remain the same. The carbon dioxide molecules thus preferred to locate near the O_Z position in MIL-127(Fe) with the distance of about 3.0 Å. It can be concluded that the sites of the lowest potential energy are in agreement with RDF results according to which the preferential adsorption site is near the O_Z positions of the metal cluster. Moreover, it can be seen

that carbon dioxide molecules are located in the center of the channel and the preferred orientation of carbon dioxide molecules is parallel to the channel of the framework.

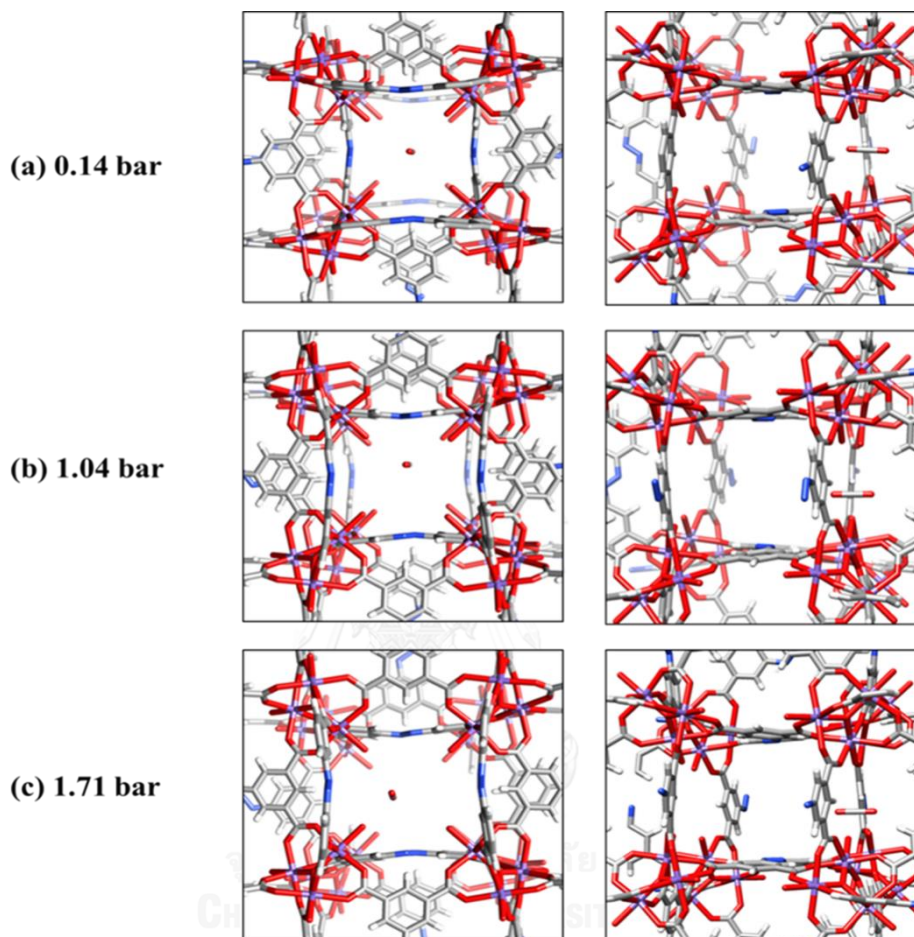


Figure 15 The position and orientation of a virtual molecule at the site and orientation of the lowest potential energy from GEMC simulations in top views (left) and side views (right) at pressure (a) 0.14 bar (top) (b) 1.04 bar (middle) and (c) 1.71 bar (bottom), are shown, respectively. The other molecules are not shown.

4.2.5 Self-Diffusion coefficient from Molecular Dynamics (MD) simulations

The particle positions were stored every 500 steps from the last 5,000,000 steps and the mean square displacement (MSD) was analysed at concentrations 1, 5, 10, 15, 20, 25 and 30 molecules/unit cell. The self-diffusion coefficients (D_s) were calculated from the slope of the MSD plot using Einstein's equation of Brownian motions. Figure

16 shows the self-diffusion coefficient of carbon dioxide at different concentrations in both the NVE and the NVT ensemble. The highest value of D_s is $3.3 \times 10^{-9} \text{ m}^2/\text{s}$ at the concentration of 10 molecules/unit cell and D_s becomes lower when the concentration is increased. At the concentration 30 molecules/unit cell, the D_s value is dropped down to $1.3 \times 10^{-9} \text{ m}^2/\text{s}$. This observation is similar to Yang et al. [77] and Chokbunpiam et al. [78], which reported the decreasing diffusivity of guest molecules with the increase of the loading at high density. This is the well-known consequence of the mutual hindrance of the guest molecules at high density.

The D_s values from NVT and NVE agree well for intermediate and high concentrations of guest molecules. This indicates that no artefact from thermalization appears. At low densities the D_s values are different. This can be understood because in the rigid lattice the thermalization by the vibrating lattice is missing. Thus, for low density the thermalization by the lattice has to be modelled by the thermostat while for higher concentrations the mutual thermalization of the guest molecules is sufficient.

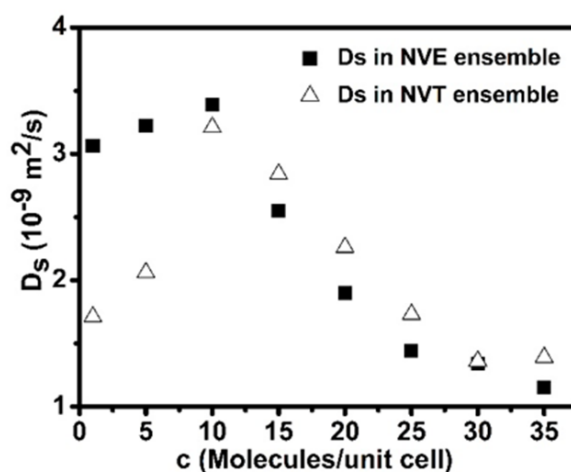


Figure 16 The self-diffusion coefficients of carbon dioxide molecules in MIL-127(Fe) at the different concentrations.

4.3 Carbon monoxide in MIL-127

4.3.1 Adsorption isotherms

The adsorption isotherms of carbon dioxide in MIL-127(Fe) show the best agreement for force field parameters that adopts LJ parameters by Babarao *et. al.* [53] for MIL-127(Fe) with the charge set 1 from QM. In this section, we continue using this parameters for MIL-12(Fe). For carbon monoxide molecules, force field parameters were taken from Palucha *et. al.* (FF1) [61], Stoll *et. al.* (FF2) [62], Straub and Karplus (FF3) [63], Sirjoosingh *et. al.* (FF4) [64] and Gu *et. al.* (FF5) [65]. The adsorption isotherm between carbon monoxide and MIL-127(Fe) with different force field parameters were shown in Fig. 17a.

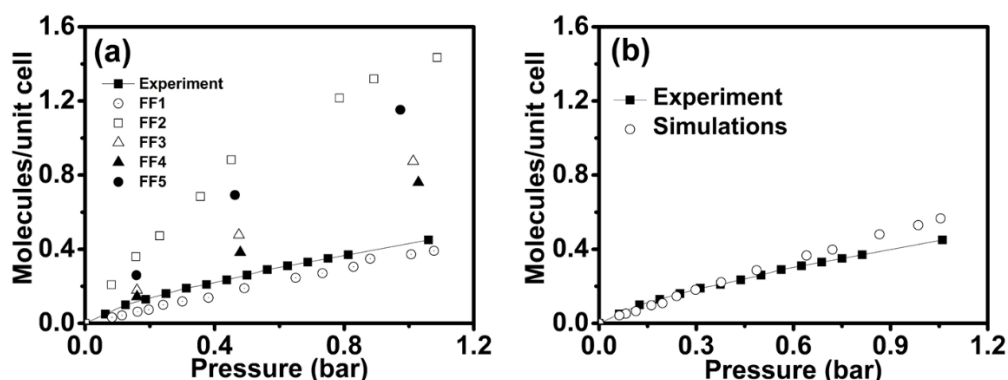


Figure 17 Adsorption isotherm of carbon monoxide in MIL-127(Fe) compared with experimental results using FF1, FF2, FF3, FF4 and FF5 for carbon monoxide and using LJ parameters from Babarao *et. al.* [53] for MIL-127(Fe) (a) and the adsorption isotherm using FF1 for carbon monoxide with applied charges (b).

The isotherm obtained by using FF1 of carbon monoxide (open circle symbol) seems to be better than FF2, FF3, FF4, FF5 when compared with the experimental results. [28] However, some suspicion occurred in the charge detail of FF1. In FF1, the charge of carbon atom is $+0.0223e$ whereas the charge of oxygen atom is $-0.0223e$. This conflict with the experiments of free carbon monoxide [66] in which the negative charge should be located at carbon atom and the positive charge should be at oxygen

atom. Therefore, we placed the charge of $-0.225e$ on carbon atom and of $+0.225e$ on oxygen atom, still using LJ potential in FF1. The adsorption isotherm with this set of charges on carbon monoxide and LJ potential in FF1 is shown in Fig. 17b. The adsorption isotherm obtained from the simulation using these parameters shows the best fit with the experimental result. Using this force field, the radial distribution function (RDF) was analysed and showed in the next part.

4.3.2 Radial Distribution Functions (RDFs)

In order to observe the preferential adsorption sites of carbon monoxide in MIL-127(Fe). RDFs were performed to analyze the closest distance between two atoms. Fig. 18 shows RDF's between the carbon monoxide and 5 atom types in MIL-127(Fe), N_N, C_O, C_N, O_Fe and O_Z, at three pressures: 0.08, 0.49, and 1.07 bar.

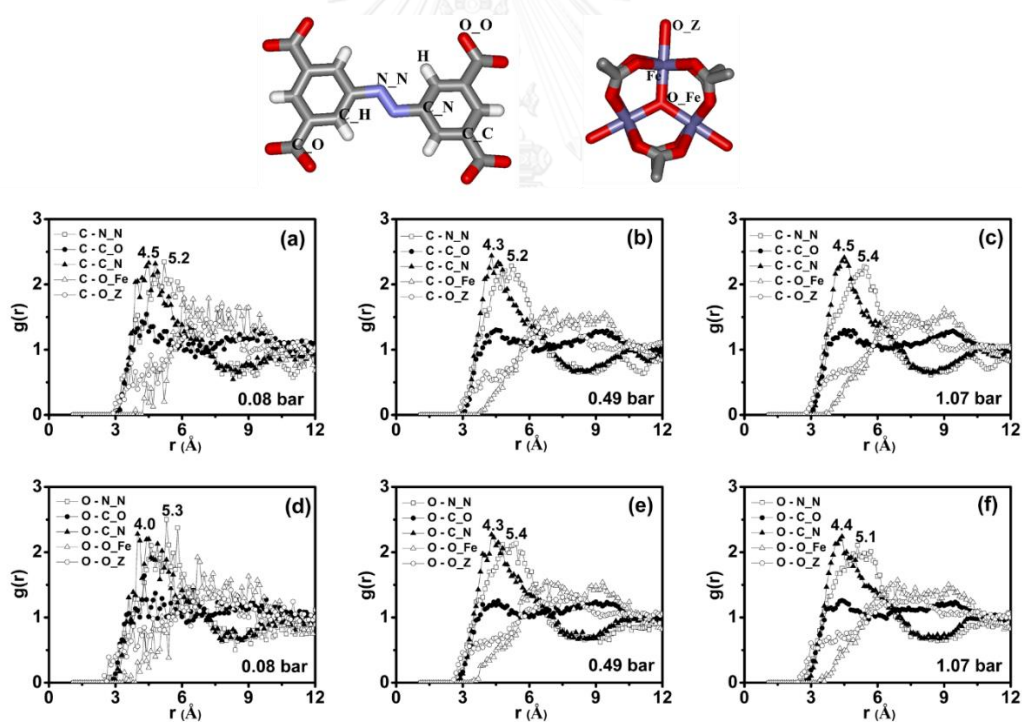


Figure 18 RDF's between carbon of carbon monoxide and 5 atom types in MIL-127(Fe) (a, b, c) and RDF between oxygen of carbon monoxide and 5 atom types in MIL-127(Fe) (d, e, f) at 0.08, 0.49, and 1.07 bar. All graphs were obtained from GEMC simulations.

RDF's for N_N, C_O, C_N, O_Fe and O_Z were represented by open square, filled circle, filled triangle, open triangle, and open circle symbols in the plots, respectively. The highest peak appear at C_N and N_N position of MIL-127(Fe) around 4 Å and 5 Å for all pressures. The O_Fe position appears around 7 Å for all pressures which show the largest distance in comparison with other atoms. This means that carbon monoxide has the weakest affinity to O_Fe similar to carbon dioxide whereas C_O and O_Z show weak interactions at all pressures. At low pressure, the peaks were fluctuated due to a few carbon monoxide molecules inside the framework. In Fig. 18, It seems to be both carbon and oxygen atom of carbon monoxide prefer to adsorb near the organic linker part, which is in contrast to carbon dioxide molecules.

4.3.3 Probability density

Fig. 19 shows the probability density of carbon monoxide inside MIL-127(Fe) in form of clouds of purple dots obtained from GEMC simulations.

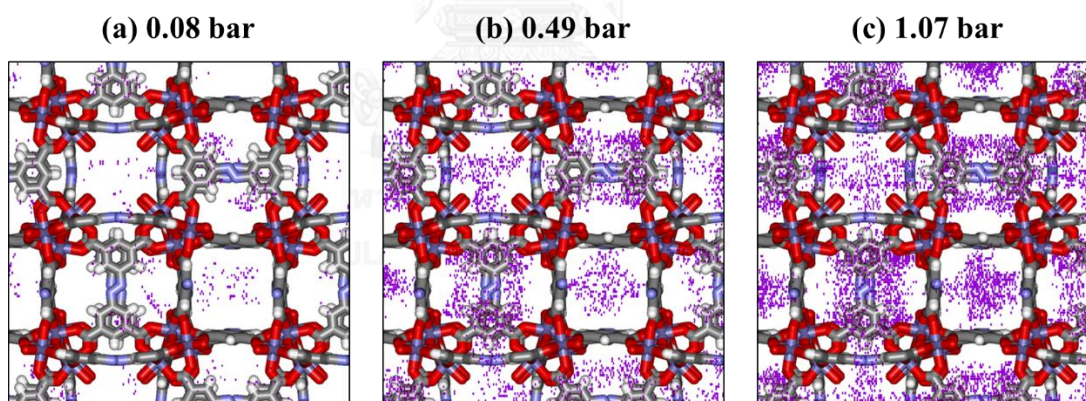


Figure 19 Probability density of carbon monoxide in MIL-127(Fe) obtained from GEMC simulations at pressure (a) 0.08 bar (b) 0.49 bar and (c) 1.07 bar, respectively.

Fig. 19a-c indicates the increase of the density of carbon monoxide as pressure increases in correspondence with the adsorption isotherm. In order to forecast the preferential adsorption site, it can be seen that CO molecules are condensed near the organic linker zone of MIL-127(Fe) more than metal cluster zone of MIL-127(Fe) at low pressures. This differs from the preferential adsorption site of CO₂, which are around

metal cluster zone of MIL-127(Fe). In addition, the probability density plot is in agreement to the RDFs which suggests the position near C_N of organic linker zone of MIL-127(Fe) to be the preferential adsorption site with the distance from CO around 4 Å.

4.3.4 Site of the lowest potential energy

Fig. 20 shows snapshots of a carbon monoxide molecule at the site corresponding to the lowest potential of the GEMC simulations at the pressure: 0.08, 0.49 and 1.07 bar, respectively. The energies of the carbon monoxide that belong to lowest potential energy are -17.936, -18.391 and -18.242 kJ/mol, respectively.

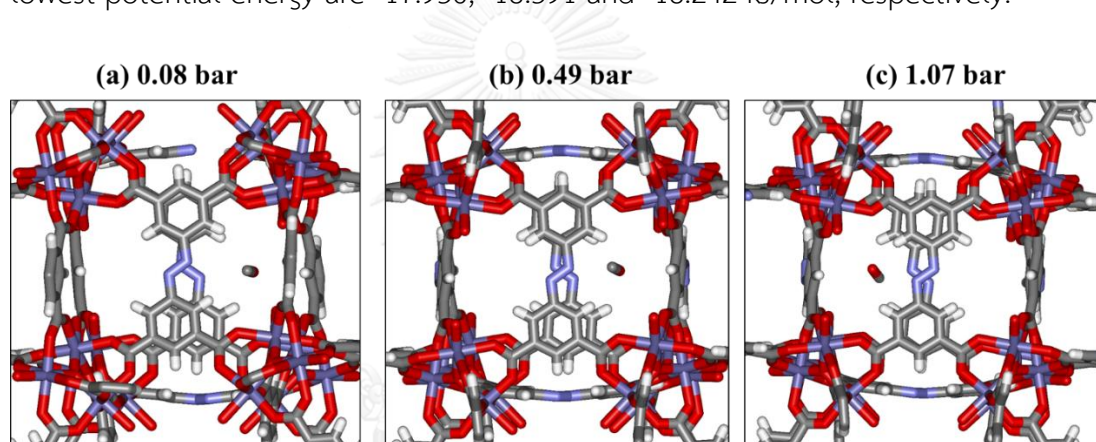


Figure 20 The position and orientation of a virtual molecule at the site and orientation of the lowest potential energy from GEMC simulations at pressure (a) 0.08 bar (b) 0.49 bar and (c) 1.07 bar, respectively. The other molecules are not shown.

From Fig. 20, the position of carbon monoxide molecule that has the lowest potential energy is near the H and C_N position of the organic linker in MIL-127(Fe) with the distance around 3 Å and 4 Å, respectively. This observation is similar to the RDFs and probability density plots. This site of CO is different from the site of lowest potential energy of CO₂ in MIL-127(Fe).

4.3.5 Self-Diffusion coefficient from Molecular Dynamics (MD) simulations

The mean square displacement (MSD) was analysed at concentrations 1, 5, 10, 15, 20, 25, 30 and 35 molecules/unit cell. The self-diffusion coefficients (D_s) were calculated from the slope of the MSD plot using Einstein's equation of Brownian motions. Figure 21 shows the self-diffusion coefficient of carbon monoxide at different concentrations in the NVT ensemble. The highest value of D_s is $13.7 \times 10^{-9} \text{ m}^2/\text{s}$ at the concentration of 7 molecules/unit cell and D_s becomes lower when the concentration is increased. At the concentration 35 molecules/unit cell, the D_s value is dropped down to $4.2 \times 10^{-9} \text{ m}^2/\text{s}$. The D_s value of CO in MIL-127 is higher than that of CO_2 at the same concentration. This result is in line with the theory of diffusion. Because the mass of CO is lower than CO_2 , so the movement of CO is faster.

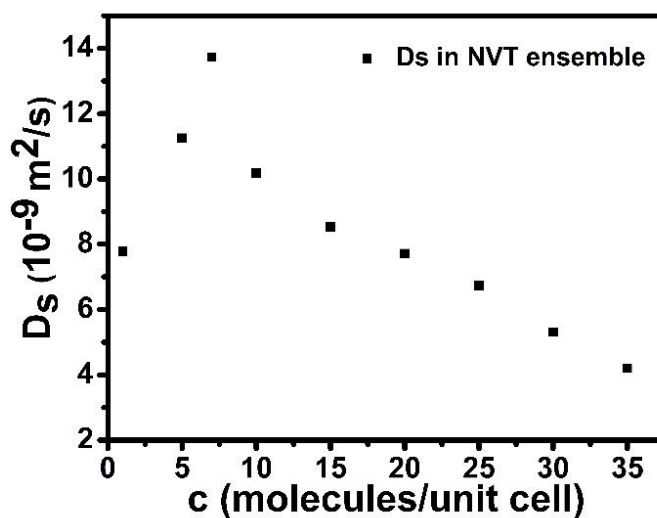


Figure 21 The self-diffusion coefficients of carbon monoxide molecules in MIL-127(Fe) at the different concentrations.

Our study shows that CO_2 can better adsorbed by MIL-127(Fe) than CO in MIL-127(Fe) material. From adsorption isotherm, it could be seen that the number of adsorbed CO_2 is higher than CO at the same pressure. Hence, MIL-127(Fe) can be used for CO/ CO_2 separation. From GEMC simulations, the preferential adsorption site of CO is near organic linker zone of MIL-127(Fe) whereas for CO_2 , it is near metal cluster zone of MIL-127(Fe). From MD simulations results, CO can diffuse faster than CO_2 in MIL-127(Fe) material owing to the self-diffusion coefficient values of CO is higher than CO_2 at the same concentrations. Thus, MIL-127(Fe) adsorbs both CO_2 and CO in the different sites and the small gases can pass through MIL-127(Fe) framework with the different velocities. Therefore, we expected that MIL-127(Fe) material can possibly using as separation of CO_2 /CO.



CHAPTER V

CONCLUSIONS

Adsorption and diffusion of small gases in MIL-127(Fe) were investigated using molecular simulations. A set of interaction parameters has been proposed for carbon dioxide and carbon monoxide in MIL-127(Fe) that well reproduces experimental adsorption data. Using rigid lattice, the adsorption isotherms between CO, CO₂ and MIL-127(Fe) were compared with the experimental results to find the most suitable force field parameters for both MIL-127(Fe) and small gases. From the Radial Distribution Functions (RDF), the shortest distance between carbon dioxide and MIL-127(Fe) was found at O_Z position of MIL-127(Fe) with the distance around 3 Å. In contrast to the RDF between MIL-127(Fe) and carbon monoxide, the shortest distance was found at the C_N position of MIL-127(Fe) with the distance around 4 Å. It can be summarized that the preferential adsorption sites of CO₂ is expected to be around the metal cluster zone of MIL-127(Fe) whereas the preferential adsorption sites of CO is expected to stay around the organic linker zone of MIL-127(Fe). In order to observe the dynamic behavior of small gases, the self-diffusivity of CO₂ was determined and it was found to be in the order of $2-3 \times 10^{-9}$ m²/s except at very high concentrations whereas the self-diffusivity of CO was found to be in the order of $4-14 \times 10^{-9}$ m²/s. For low concentrations the diffusivity increases slightly with increasing concentration while at higher concentrations it decreases as a consequence of mutual hindrance of the guest molecules. The comparison of simulations in the NVT and the NVE ensembles suggests that for simulations with rigid lattice at low densities a thermostat is needed, while at higher loadings the mutual thermalization of the guest molecules can well replace the thermostat.

REFERENCES

- [1] Khoo, H.H. and Tan, R.B.H. Life Cycle Investigation of CO₂ Recovery and Sequestration. Environmental Science & Technology 40(12) (2006): 4016-4024.
- [2] Rao, A.B. and Rubin, E.S. A Technical, Economic, and Environmental Assessment of Amine-Based CO₂ Capture Technology for Power Plant Greenhouse Gas Control. Environmental Science & Technology 36(20) (2002): 4467-4475.
- [3] Janiak, C. and Vieth, J.K. MOFs, MILs and more: concepts, properties and applications for porous coordination networks (PCNs). New Journal of Chemistry 34(11) (2010): 2366-2388.
- [4] Yang, Q., Xue, C., Zhong, C., and Chen, J.-F. Molecular simulation of separation of CO₂ from flue gases in CU-BTC metal-organic framework. AIChE Journal 53(11) (2007): 2832-2840.
- [5] Ramsahye, N.A., et al. Adsorption of CO₂ in metal organic frameworks of different metal centres: Grand Canonical Monte Carlo simulations compared to experiments. Adsorption 13(5) (2007): 461-467.
- [6] Chokbunpiam, T., Fritzsche, S., Chmelik, C., Caro, J., Janke, W., and Hannongbua, S. Gate opening effect for carbon dioxide in ZIF-8 by molecular dynamics – Confirmed, but at high CO₂ pressure. Chemical Physics Letters 648 (2016): 178-181.
- [7] Chokbunpiam, T., et al. The importance of lattice flexibility for the migration of ethane in ZIF-8: Molecular dynamics simulations. Microporous and Mesoporous Materials 174 (2013): 126-134.
- [8] Phuong, V.T., et al. Methane in zeolitic imidazolate framework ZIF-90: Adsorption and diffusion by molecular dynamics and Gibbs ensemble Monte Carlo. Microporous and Mesoporous Materials 235 (2016): 69-77.

- [9] Babarao, R. and Jiang, J. Diffusion and Separation of CO₂ and CH₄ in Silicalite, C168 Schwarzite, and IRMOF-1: A Comparative Study from Molecular Dynamics Simulation. Langmuir 24(10) (2008): 5474-5484.
- [10] Skoulidas, A.I. and Sholl, D.S. Self-Diffusion and Transport Diffusion of Light Gases in Metal-Organic Framework Materials Assessed Using Molecular Dynamics Simulations. The Journal of Physical Chemistry B 109(33) (2005): 15760-15768.
- [11] Li, J.-R., Sculley, J., and Zhou, H.-C. Metal–Organic Frameworks for Separations. Chemical Reviews 112(2) (2012): 869-932.
- [12] Zhu, Q.-L. and Xu, Q. Metal-organic framework composites. Chemical Society Reviews 43(16) (2014): 5468-5512.
- [13] Ferey, G. Hybrid porous solids: past, present, future. Chemical Society Reviews 37(1) (2008): 191-214.
- [14] Li, J.-R., Kuppler, R.J., and Zhou, H.-C. Selective gas adsorption and separation in metal-organic frameworks. Chemical Society Reviews 38(5) (2009): 1477-1504.
- [15] Horcajada, P., et al. Metal–Organic Frameworks in Biomedicine. Chemical Reviews 112(2) (2012): 1232-1268.
- [16] Furukawa, H., Cordova, K.E., O’Keeffe, M., and Yaghi, O.M. The Chemistry and Applications of Metal-Organic Frameworks. Science 341(6149) (2013).
- [17] Gangu, K.K., Maddila, S., Mukkamala, S.B., and Jonnalagadda, S.B. A review on contemporary Metal–Organic Framework materials. Inorganica Chimica Acta 446 (2016): 61-74.
- [18] Morris, R.E. and Wheatley, P.S. Gas Storage in Nanoporous Materials. Angewandte Chemie International Edition 47(27) (2008): 4966-4981.

- [19] Latroche, M., et al. Hydrogen Storage in the Giant-Pore Metal–Organic Frameworks MIL-100 and MIL-101. Angewandte Chemie International Edition 45(48) (2006): 8227-8231.
- [20] Castillo, J.M., Vlugt, T.J.H., and Calero, S. Molecular Simulation Study on the Separation of Xylene Isomers in MIL-47 Metal–Organic Frameworks. The Journal of Physical Chemistry C 113(49) (2009): 20869-20874.
- [21] Santiago-Portillo, A., Navalón, S., Cirujano, F.G., Xamena, F.X.L.i., Alvaro, M., and Garcia, H. MIL-101 as Reusable Solid Catalyst for Autoxidation of Benzylic Hydrocarbons in the Absence of Additional Oxidizing Reagents. ACS Catalysis 5(6) (2015): 3216-3224.
- [22] McNamara, N.D., Neumann, G.T., Masko, E.T., Urban, J.A., and Hicks, J.C. Catalytic performance and stability of (V) MIL-47 and (Ti) MIL-125 in the oxidative desulfurization of heterocyclic aromatic sulfur compounds. Journal of Catalysis 305 (2013): 217-226.
- [23] Horcajada, P., et al. Synthesis and catalytic properties of MIL-100 (Fe), an iron (III) carboxylate with large pores. Chemical Communications (27) (2007): 2820-2822.
- [24] Dhakshinamoorthy, A., et al. Iron(iii) metal-organic frameworks as solid Lewis acids for the isomerization of [small alpha]-pinene oxide. Catalysis Science & Technology 2(2) (2012): 324-330.
- [25] Liu, Y., et al. Assembly of metal-organic frameworks (MOFs) based on indium-trimer building blocks: a porous MOF with soc topology and high hydrogen storage. Angew Chem Int Ed Engl 46(18) (2007): 3278-83.
- [26] Cunha, D., et al. Rationale of Drug Encapsulation and Release from Biocompatible Porous Metal–Organic Frameworks. Chemistry of Materials 25(14) (2013): 2767-2776.
- [27] Eubank, J.F., et al. Porous, rigid metal(III)-carboxylate metal-organic frameworks for the delivery of nitric oxide. APL Mater. 2(12) (2014): 124112.

- [28] Wongsakulphasatch, S., et al. Direct accessibility of mixed-metal (III/II) acid sites through the rational synthesis of porous metal carboxylates. Chem Commun (Camb) 51(50) (2015): 10194-7.
- [29] Chevreau, H., et al. Synthesis of the biocompatible and highly stable MIL-127(Fe): from large scale synthesis to particle size control. CrystEngComm 18(22) (2016): 4094-4101.
- [30] McQuarrie, D.A. Quantum chemistry. University Science Books, 2008.
- [31] Schrödinger, E. An Undulatory Theory of the Mechanics of Atoms and Molecules. Physical Review 28(6) (1926): 1049-1070.
- [32] Lewars, E.G. Introduction to Quantum Mechanics in Computational Chemistry. in Computational Chemistry: Introduction to the Theory and Applications of Molecular and Quantum Mechanics, pp. 85-173. Dordrecht: Springer Netherlands, 2011.
- [33] Sherrill, C.D. The born-oppenheimer approximation. School of Chemistry and Biochemistry, Georgia Institute of Technology (2005).
- [34] Szabo, A. and Ostlund, N.S. Modern quantum chemistry: introduction to advanced electronic structure theory. Courier Corporation, 1989.
- [35] Sherrill, C.D. An introduction to Hartree-Fock molecular orbital theory. School of Chemistry and Biochemistry Georgia Institute of Technology (2000).
- [36] Huzinaga, S. Basis sets for molecular calculations. Computer Physics Reports 2(6) (1985): 281-339.
- [37] Hill, T.L. An introduction to statistical thermodynamics. Courier Corporation, 2012.
- [38] Li, C. and Chou, T.-W. A structural mechanics approach for the analysis of carbon nanotubes. International Journal of Solids and Structures 40(10) (2003): 2487-2499.

- [39] OpenWetWare. Biomod/2013/NanoUANL/Simulations [Online]. Available from: <http://openwetware.org/index.php?title=Biomod/2013/NanoUANL/Simulations&oldid=749784> [12 December 2016]
- [40] Panagiotopoulos, A.Z. Direct determination of phase coexistence properties of fluids by Monte Carlo simulation in a new ensemble. Molecular Physics 61(4) (1987): 813-826.
- [41] Chen, B., Siepmann, J.I., and Klein, M.L. Direct Gibbs Ensemble Monte Carlo Simulations for Solid–Vapor Phase Equilibria: Applications to Lennard–Jonesium and Carbon Dioxide. The Journal of Physical Chemistry B 105(40) (2001): 9840-9848.
- [42] Panagiotopoulos, A.Z., Quirke, N., Stapleton, M., and Tildesley, D.J. Phase equilibria by simulation in the Gibbs ensemble. Molecular Physics 63(4) (1988): 527-545.
- [43] Côté, A.S., Smith, B., and Lindan, P.J.D. [Online]. Available from: <http://www.compsoc.man.ac.uk/~lucky/Democritus/Theory/pbc-mi.html>
- [44] Allen, M.P. Introduction to molecular dynamics simulation.
- [45] Roux, S.L. and Petkova, V. Interactive Structure Analysis of Amorphous and Crystalline Systems [Online]. Available from: <http://isaacs.sourceforge.net/phys/rdfs.html#gr-fig>
- [46] Wang, J. and Hou, T. Application of molecular dynamics simulations in molecular property prediction II: diffusion coefficient. Journal of computational chemistry 32(16) (2011): 3505-3519.
- [47] Mulliken, R.S. Electronic Population Analysis on LCAO-MO Molecular Wave Functions. I. Journal of Chemical Physics 23 (1955): 1833-1840.

- [48] Campaña, C., Mussard, B., and Woo, T.K. Electrostatic Potential Derived Atomic Charges for Periodic Systems Using a Modified Error Functional. Journal of Chemical Theory and Computation 5(10) (2009): 2866-2878.
- [49] Breneman, C.M. and Wiberg, K.B. Determining atom-centered monopoles from molecular electrostatic potentials. The need for high sampling density in formamide conformational analysis. Journal of Computational Chemistry 11(3) (1990): 361-373.
- [50] Frisch, M.J., et al. Gaussian09, Revision A11. 4, Gaussian. Inc., Pittsburgh, PA (2008).
- [51] Rappe, A.K., Casewit, C.J., Colwell, K.S., Goddard, W.A., and Skiff, W.M. UFF, a full periodic table force field for molecular mechanics and molecular dynamics simulations. Journal of the American Chemical Society 114(25) (1992): 10024-10035.
- [52] Mayo, S.L., Olafson, B.D., and Goddard, W.A. DREIDING: a generic force field for molecular simulations. The Journal of Physical Chemistry 94(26) (1990): 8897-8909.
- [53] Babarao, R. and Jiang, J. Molecular Screening of Metal–Organic Frameworks for CO₂ Storage. Langmuir 24(12) (2008): 6270-6278.
- [54] Potoff, J.J. and Siepmann, J.I. Vapor–liquid equilibria of mixtures containing alkanes, carbon dioxide, and nitrogen. AIChE Journal 47(7) (2001): 1676-1682.
- [55] Liu, D., Wu, Y., Xia, Q., Li, Z., and Xi, H. Experimental and molecular simulation studies of CO₂ adsorption on zeolitic imidazolate frameworks: ZIF-8 and amine-modified ZIF-8. Adsorption 19(1) (2013): 25-37.
- [56] Goj, A., Sholl, D.S., Akten, E.D., and Kohen, D. Atomistic Simulations of CO₂ and N₂ Adsorption in Silica Zeolites: The Impact of Pore Size and Shape. The Journal of Physical Chemistry B 106(33) (2002): 8367-8375.
- [57] García-Pérez, E., et al. A computational study of CO₂, N₂, and CH₄ adsorption in zeolites. Adsorption 13(5) (2007): 469-476.

- [58] Do, D.D. and Do, H.D. Effects of potential models on the adsorption of carbon dioxide on graphitized thermal carbon black: GCMC computer simulations. Colloids and Surfaces A: Physicochemical and Engineering Aspects 277(1–3) (2006): 239-248.
- [59] Merz, K.M. Carbon dioxide binding to human carbonic anhydrase II. Journal of the American Chemical Society 113(2) (1991): 406-411.
- [60] Babarao, R., Jiang, J., and Sandler, S.I. Molecular Simulations for Adsorptive Separation of CO₂/CH₄ Mixture in Metal-Exposed, Catenated, and Charged Metal–Organic Frameworks. Langmuir 25(9) (2009): 5239-5247.
- [61] Pałucha, S., Gburski, Z., and Biesiada, J. A molecular dynamics study of fullerene–carbon monoxide mixture. Journal of molecular structure 704(1) (2004): 269-273.
- [62] Stoll, J., Vrabec, J., and Hasse, H. A set of molecular models for carbon monoxide and halogenated hydrocarbons. The Journal of chemical physics 119(21) (2003): 11396-11407.
- [63] Straub, J.E. and Karplus, M. Molecular dynamics study of the photodissociation of carbon monoxide from myoglobin: ligand dynamics in the first 10 ps. Chemical physics 158(2) (1991): 221-248.
- [64] Sirjoosingh, A., Alavi, S., and Woo, T.K. Grand-canonical Monte Carlo and molecular-dynamics simulations of carbon-dioxide and carbon-monoxide adsorption in zeolitic imidazolate framework materials. The Journal of Physical Chemistry C 114(5) (2010): 2171-2178.
- [65] Gu, C., Gao, G.-H., Yu, Y.-X., and Nitta, T. Simulation for separation of hydrogen and carbon monoxide by adsorption on single-walled carbon nanotubes. Fluid Phase Equilibria 194 (2002): 297-307.
- [66] Scuseria, G.E., Miller, M.D., Jensen, F., and Geertsen, J. The dipole moment of carbon monoxide. The Journal of chemical physics 94(10) (1991): 6660-6663.

- [67] Allen, M.P. and Tildesley, D.J. Computer simulation of liquids. Oxford university press, 1989.
- [68] Landau, D.P. and Binder., K. A Guide to Monte Carlo Simulations in Statistical Physics. Cambridge University Press, 2009.
- [69] Yazaydin, A.Ö., et al. Screening of Metal–Organic Frameworks for Carbon Dioxide Capture from Flue Gas Using a Combined Experimental and Modeling Approach. Journal of the American Chemical Society 131(51) (2009): 18198-18199.
- [70] van Gunsteren, W.F. and Berendsen, H.J.C. Computer Simulation of Molecular Dynamics: Methodology, Applications, and Perspectives in Chemistry. Angewandte Chemie International Edition in English 29(9) (1990): 992-1023.
- [71] Peng, D.-Y. and Robinson, D.B. A New Two-Constant Equation of State. Industrial & Engineering Chemistry Fundamentals 15(1) (1976): 59-64.
- [72] Smith, W. and Todorov, I.T. A short description of DL_POLY. Molecular Simulation 32(12-13) (2006): 935-943.
- [73] Posch, H.A., Hoover, W.G., and Vesely, F.J. Canonical dynamics of the Nosé oscillator: Stability, order, and chaos. Physical Review A 33(6) (1986): 4253-4265.
- [74] Legoll, F., Luskin, M., and Moeckel, R. Non-Ergodicity of the Nosé–Hoover Thermostatted Harmonic Oscillator. Archive for Rational Mechanics and Analysis 184(3) (2007): 449-463.
- [75] Harvey, S.C., Tan, R.K.Z., and Cheatham, T.E. The flying ice cube: Velocity rescaling in molecular dynamics leads to violation of energy equipartition. Journal of Computational Chemistry 19(7) (1998): 726-740.
- [76] Fritzsche, S., Haberlandt, R., Kaerger, J., Pfeifer, H., and Wolfsberg, M. Molecular dynamics consideration of the mutual thermalization of guest molecules in zeolites. Chemical Physics Letters 171(1) (1990): 109-113.

- [77] Yang, Q., Zhong, C., and Chen, J.-F. Computational Study of CO₂ Storage in Metal–Organic Frameworks. The Journal of Physical Chemistry C 112(5) (2008): 1562-1569.
- [78] Chokbunpiam, T., et al. N₂ in ZIF-8: Sorbate induced structural changes and self-diffusion. Microporous and Mesoporous Materials 187 (2014): 1-6.



APPENDIX

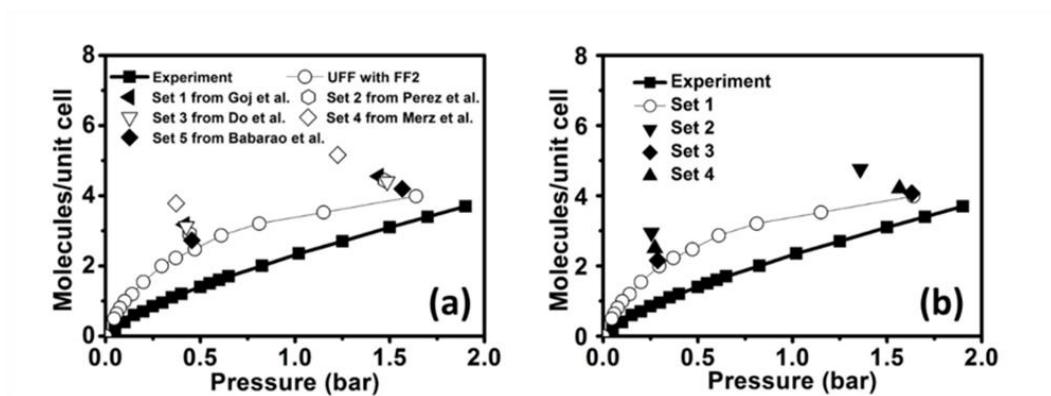


Figure 22 Adsorption isotherm between MIL-127(Fe) and carbon dioxide compared with experiment. (a) After adjusted the charge of CO_2 , (b) after adjusted the charge of MIL-127(Fe).

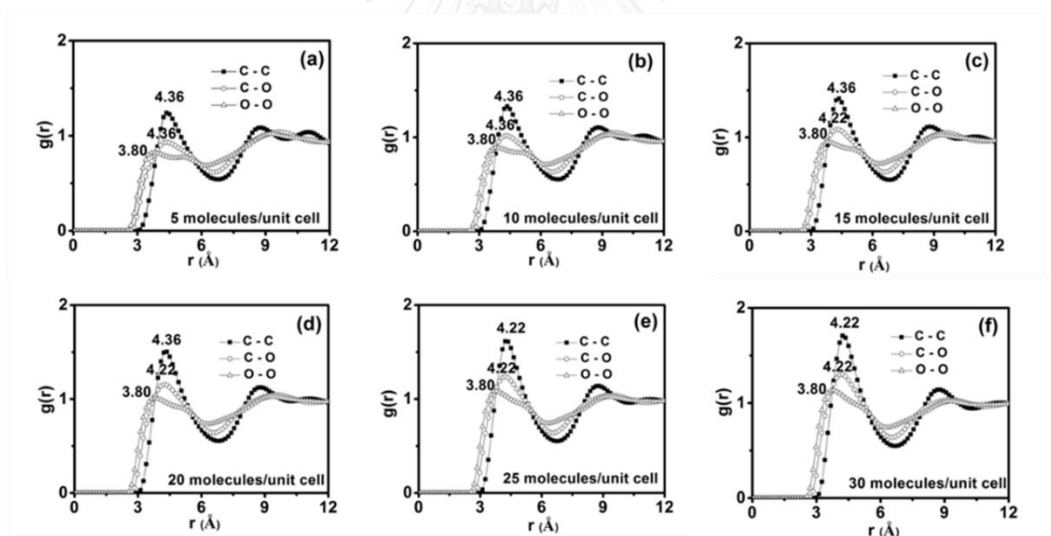


Figure 23 RDF of carbon dioxide in MIL-127(Fe) at concentration 5, 10, 15, 20, 25 and 30 molecules/unit cell, respectively. All graphs obtained from MD simulations.

Table 7 The calculated electrostatic potential (ESP) charges to estimate the atomic partial charge in each atom types.

Number	atom	ESP charges	Number	Atom	ESP charges
1	O	-0.797668	27	H	0.000000
2	O	-0.796235	28	H	0.000000
3	O	-0.796066	29	C	0.372897
4	O	-0.794023	30	C	0.342238
5	O	-0.893554	31	N	-0.187457
6	O	-0.888890	32	N	-0.225521
7	O	-0.891117	33	O	-1.012465
8	O	-0.888588	34	O	-1.183421
9	C	0.827257	35	O	-0.853708
10	C	0.823432	36	Fe	2.013106
11	C	-0.118999	37	O	-0.916850
12	C	-0.113947	38	O	-1.388126
13	H	0.000000	39	Fe	1.923616
14	H	0.000000	40	O	-0.562301
15	C	-0.234674	41	O	-0.902857
16	C	-0.201023	42	O	-1.176557
17	H	0.000000	43	O	-1.212168
18	H	0.000000	44	H	0.000000
19	C	0.064239	45	H	0.000000
20	C	0.050533	46	H	0.000000
21	C	0.855356	47	H	0.000000
22	C	0.845535	48	H	0.000000
23	C	-0.030172	49	H	0.000000
24	C	-0.020639	50	H	0.000000
25	C	-0.149526	51	O	-0.728268
26	C	-0.153389	52	H	0.000000

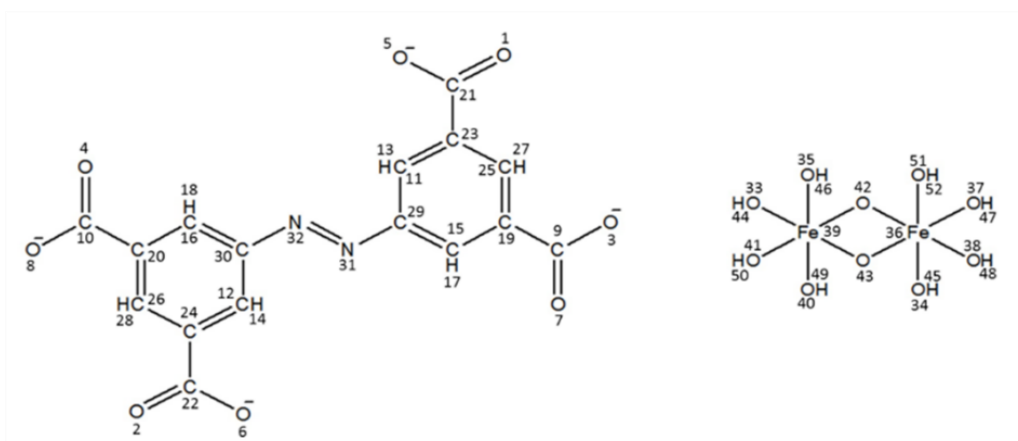


Figure 24 Two structures used to estimate the electrostatic potential (ESP) charges for organic linker (left) and metal cluster (right) in MIL-127(Fe).

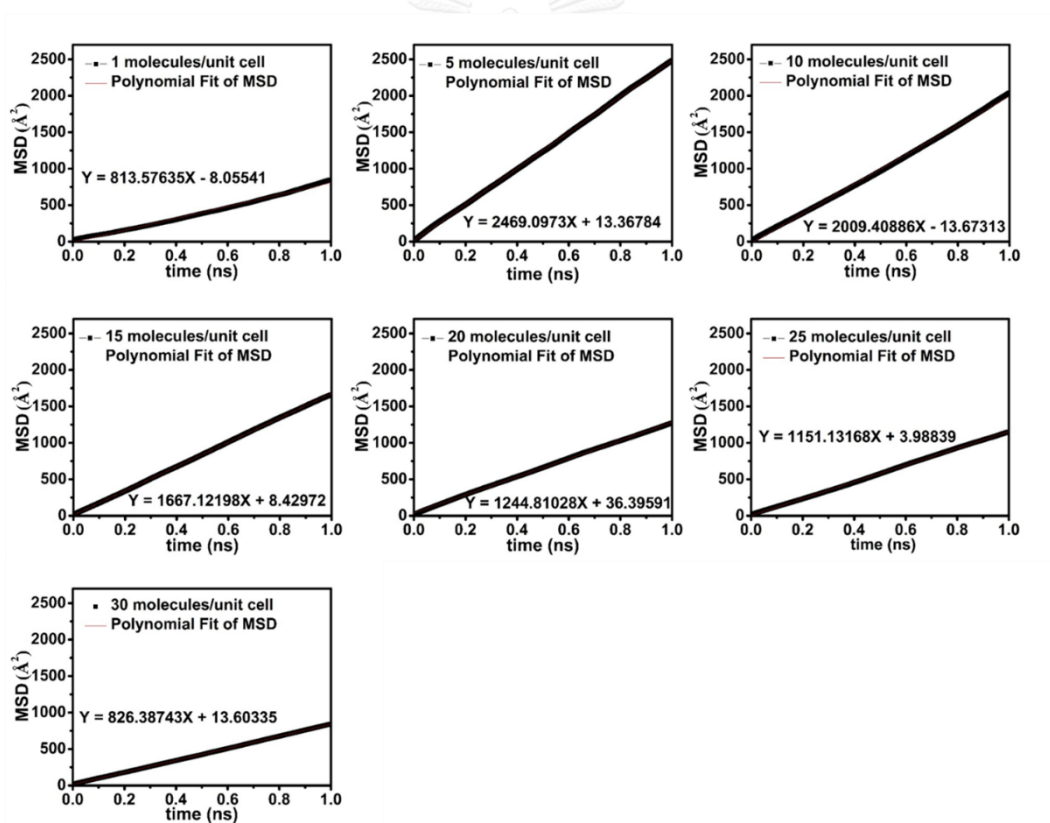


Figure 25 The mean square displacement of carbon dioxide in MIL-127(Fe) obtained from NVT ensemble.

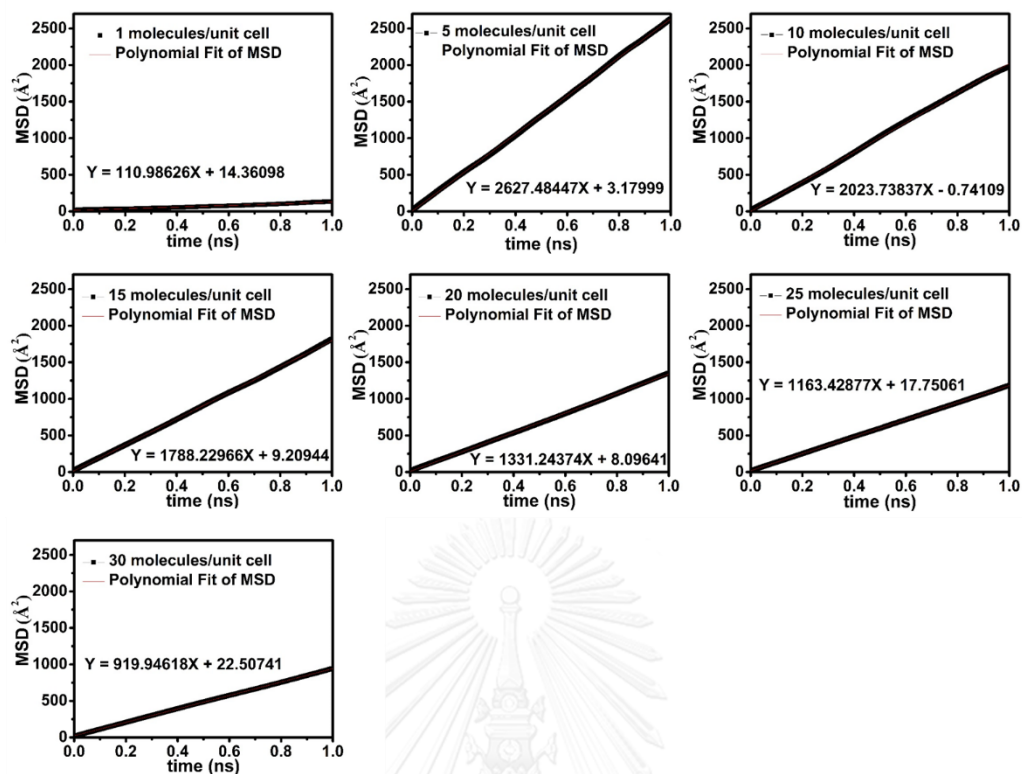
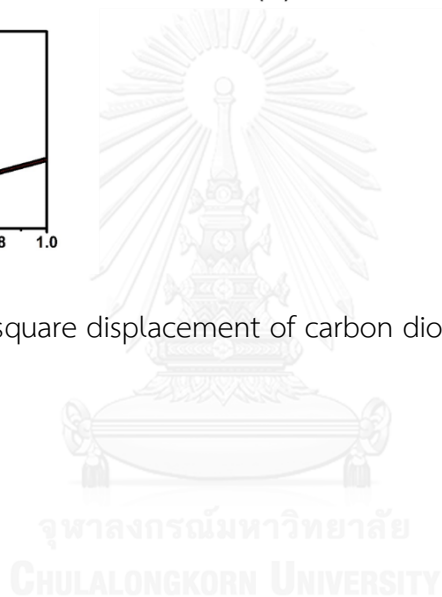


Figure 26 The mean square displacement of carbon dioxide in MIL-127(Fe) obtained from NVE ensemble.



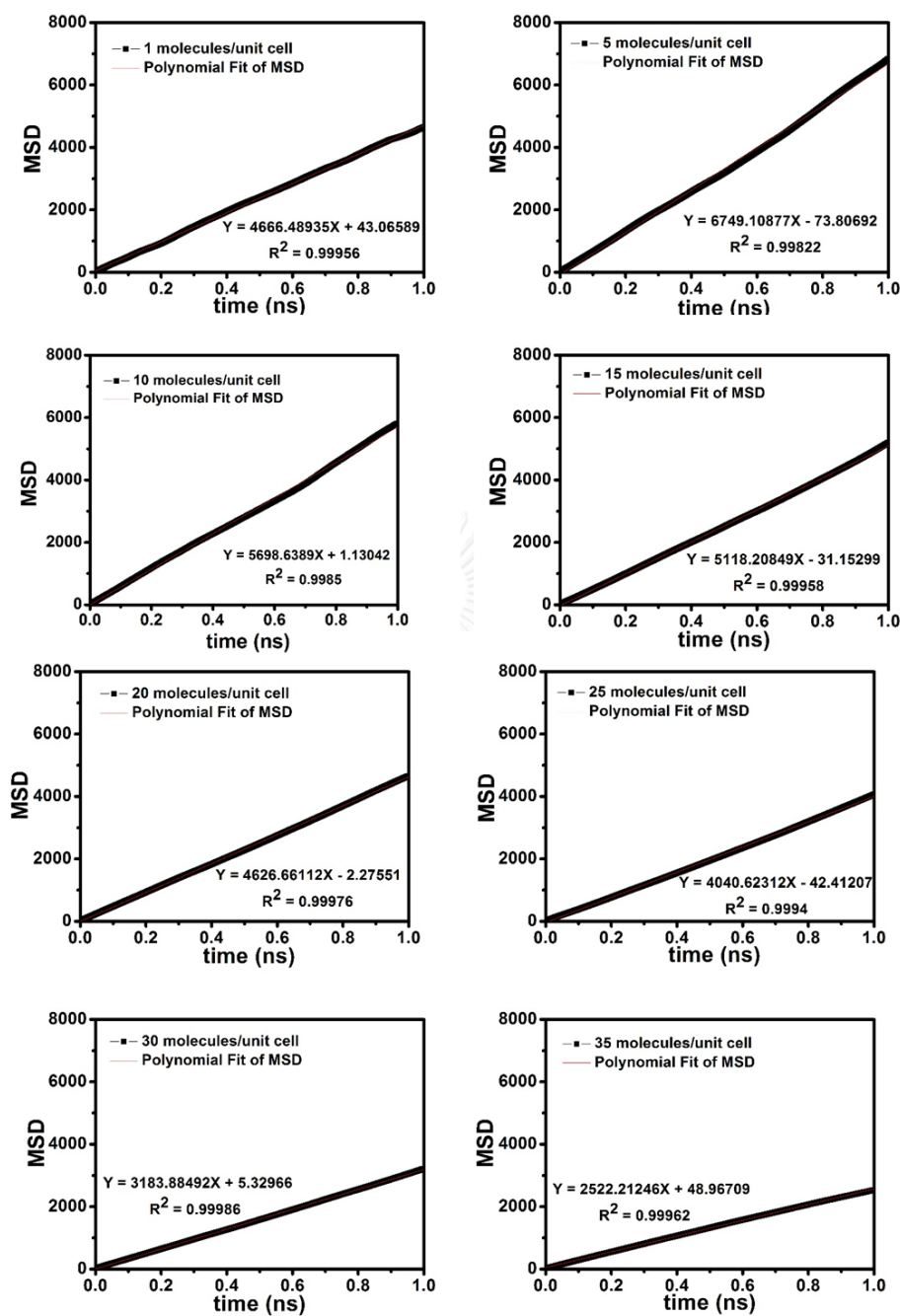


Figure 27 The mean square displacement of carbon monoxide in MIL-127(Fe) obtained from NVT ensemble.

VITA

Name: Mr. Pavee Pongsajanukul

Date of birth: 27th June 1991

Email: pavee_pongsajanukul@hotmail.com

Educations:

2004-2009: Surawittayakarn School, Surin

2010-2013: Bachelor of Science, Department of Chemistry, Faculty of Science, Khon Kaen University, Khon Kaen (Second class honors)

2014-present: Master of Science, Department of Chemistry, Faculty of Science, Chulalongkorn University, Bangkok

Experiences:

- Poster presentation in The 13th Thai Summer School of Computational Chemistry 2016, Chiang Mai

- Poster presentation and staff in Pure and Applied Chemistry International Conference (PACCON) 2016, Bangkok

- Oral and poster presentation in Pure and Applied Chemistry International Conference (PACCON) 2014, Bangkok